

Structure-Based Design of Orally Bioavailable 1*H*-Pyrrolo[3,2-*c*]pyridine Inhibitors of Mitotic Kinase Monopolar Spindle 1 (MPS1)

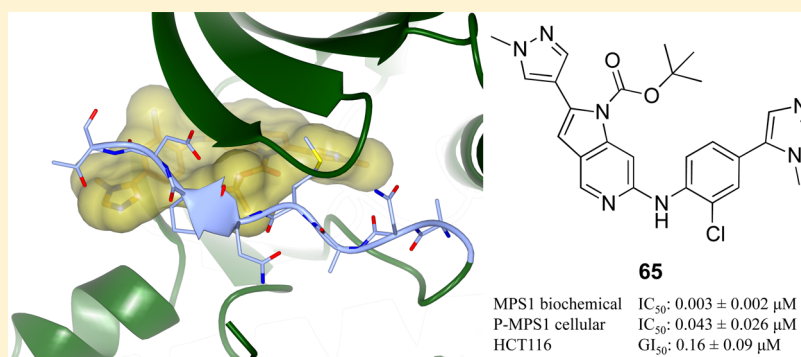
Sébastien Naud,[†] Isaac M. Westwood,^{†,‡} Amir Faisal,[†] Peter Sheldrake,[†] Vassilios Bavetsias,[†] Butrus Atrash,[†] Kwai-Ming J. Cheung,[†] Manjuan Liu,[†] Angela Hayes,[†] Jessica Schmitt,[†] Amy Wood,[†] Vanessa Choi,[†] Kathy Boxall,[†] Grace Mak,[†] Mark Gurden,[§] Melanie Valenti,[†] Alexis de Haven Brandon,[†] Alan Henley,[†] Ross Baker,[†] Craig McAndrew,[†] Berry Matijssen,[†] Rosemary Burke,[†] Swen Hoelder,[†] Suzanne A. Eccles,[†] Florence I. Raynaud,[†] Spiros Linardopoulos,^{†,§} Rob L. M. van Montfort,^{*,†,‡} and Julian Blagg^{*,†}

[†]Cancer Research UK Cancer Therapeutics Unit, Division of Cancer Therapeutics, The Institute of Cancer Research, London SM2 5NG, United Kingdom

[‡]Division of Structural Biology, The Institute of Cancer Research, London SW3 6JB, United Kingdom

[§]The Breakthrough Breast Cancer Research Centre, Division of Breast Cancer Research, The Institute of Cancer Research, London SW3 6JB, United Kingdom

S Supporting Information



ABSTRACT: The protein kinase MPS1 is a crucial component of the spindle assembly checkpoint signal and is aberrantly overexpressed in many human cancers. MPS1 is one of the top 25 genes overexpressed in tumors with chromosomal instability and aneuploidy. PTEN-deficient breast tumor cells are particularly dependent upon MPS1 for their survival, making it a target of significant interest in oncology. We report the discovery and optimization of potent and selective MPS1 inhibitors based on the 1*H*-pyrrolo[3,2-*c*]pyridine scaffold, guided by structure-based design and cellular characterization of MPS1 inhibition, leading to **65** (CCT251455). This potent and selective chemical tool stabilizes an inactive conformation of MPS1 with the activation loop ordered in a manner incompatible with ATP and substrate-peptide binding; it displays a favorable oral pharmacokinetic profile, shows dose-dependent inhibition of MPS1 in an HCT116 human tumor xenograft model, and is an attractive tool compound to elucidate further the therapeutic potential of MPS1 inhibition.

INTRODUCTION

The main role of the cell cycle is to enable error-free DNA replication, chromosome segregation, and cytokinesis. Surveillance mechanisms, the checkpoint pathways, monitor passage through the cell cycle at several stages. During mitosis, the spindle assembly checkpoint (SAC) prevents anaphase onset until the appropriate tension and attachment across kinetochores is achieved.^{1,2} One of the first components of the SAC signal, identified by a genetic screen in budding yeast, was dubbed MPS1 (monopolar spindle 1, also known as TTK) because of the monopolar spindles produced by MPS1 mutant cells.³ Subsequently, the MPS1 gene was shown to encode an essential

dual-specificity kinase conserved from yeast to humans.^{4,5} MPS1 activity peaks at the G2/M transition, is enhanced upon activation of the SAC with nocodazole,⁶ and is dependent upon autophosphorylation of a threonine at position 676 in the activation loop.⁷ MPS1 is required for normal function of the mitotic spindle checkpoint and subsequent cell division; it is aberrantly overexpressed in a wide range of human tumors including bladder, anaplastic thyroid, breast, lung, esophagus, and prostate cancers.^{8–12} In addition, MPS1 has been identified in the

Received: September 10, 2013

Published: November 20, 2013

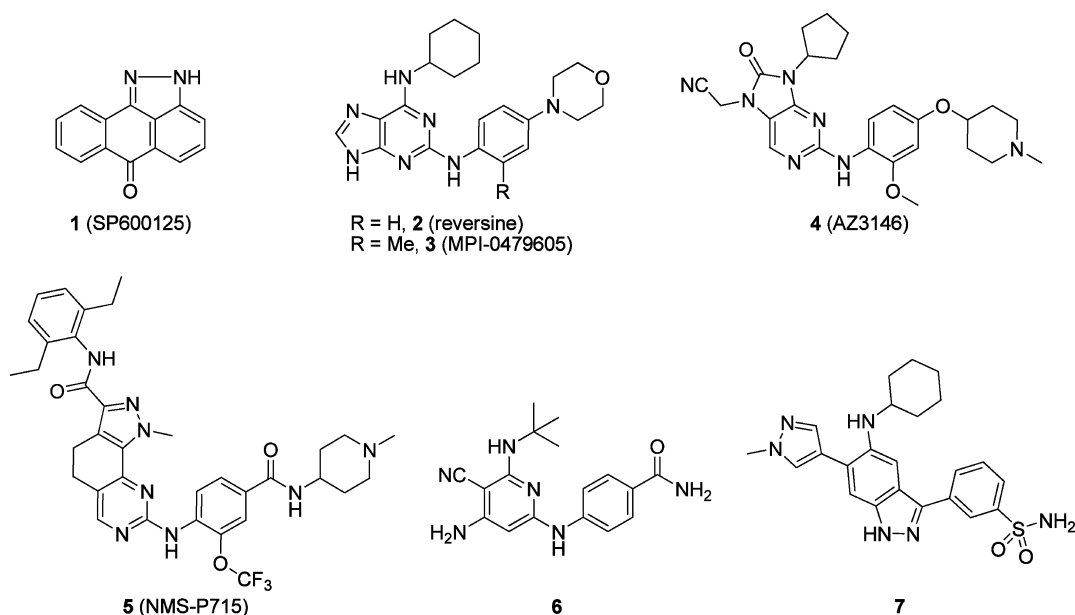


Figure 1. Small-molecule MPS1 inhibitors 1,^{16–18} 2,¹⁹ 3,²² 4,²³ 5,^{24,25} 6,²⁶ and 7.²⁷

signature of the top 25 genes overexpressed in tumors with chromosomal instability¹³ and aneuploidy,^{14,15} with PTEN-deficient breast tumor cells particularly dependent upon MPS1 for their survival such that RNAi-mediated knockdown or chemical inhibition of MPS1 leads to cell death.¹⁴ This body of work has engendered significant interest in the discovery of selective small-molecule chemical tools to elucidate further the therapeutic potential of MPS1 inhibition for the treatment of cancer.

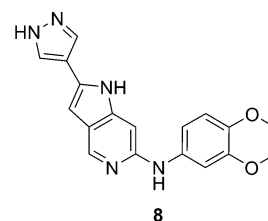
First-generation nonselective inhibitors of MPS1 have been described, for example, 1 (SP600125), a JNK (c-Jun amino-terminal kinase) inhibitor that disrupts SAC function in a JNK-independent manner via the inhibition of MPS1,^{16–18} and 2 (reversine), an MPS1, Aurora A, and Aurora B inhibitor.¹⁹ More recently, several selective small-molecule MPS1 inhibitors have been utilized to explore the cellular function of MPS1.^{20,21} These include 3 (MPI-0479605),²² 4 (AZ3146),²³ 5 (NMS-P715),^{24,25} a series of selective diaminopyridine-based inhibitors exemplified by 6²⁶ that demonstrates inhibition of growth of A549 human tumor xenografts, and a set of indazole-based inhibitors represented by 7²⁷ (Figure 1).

Here, we describe the discovery of orally bioavailable small-molecule inhibitors of MPS1 based on the 1*H*-pyrrolo[3,2-*c*]pyridine scaffold in a medicinal-chemistry program enabled by structure-based design and cellular characterization of MPS1 inhibition. We show that optimized compounds in this series display potent and selective inhibition of MPS1 *in vitro* and translate well to cellular assays of MPS1 autophosphorylation and antiproliferative activity when compared to other recently reported MPS1 inhibitors. We also show, by X-ray crystallographic studies, that exemplars of this series stabilize an inactive conformation of MPS1 in which the activation loop is ordered in a manner incompatible with ATP and substrate-peptide binding.

Our starting point was the potent but nonselective and metabolically unstable compound 8 identified in a high-throughput screen of an in-house kinase-focused compound library (Figure 2).

CHEMISTRY

Our synthetic strategy to all desired 1*H*-pyrrolo[3,2-*c*]pyridines involved palladium-mediated Sonagashira coupling of an appropriately substituted 4-amino-2-bromo-5-iodopyridine, 9,



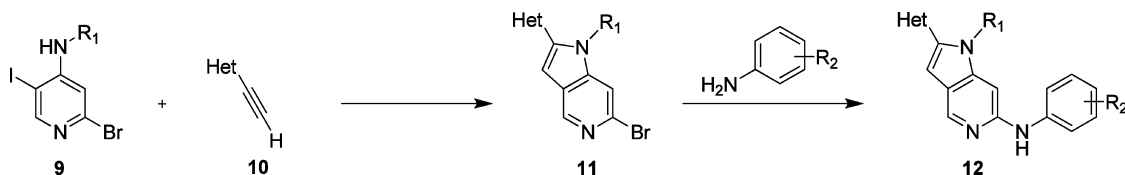
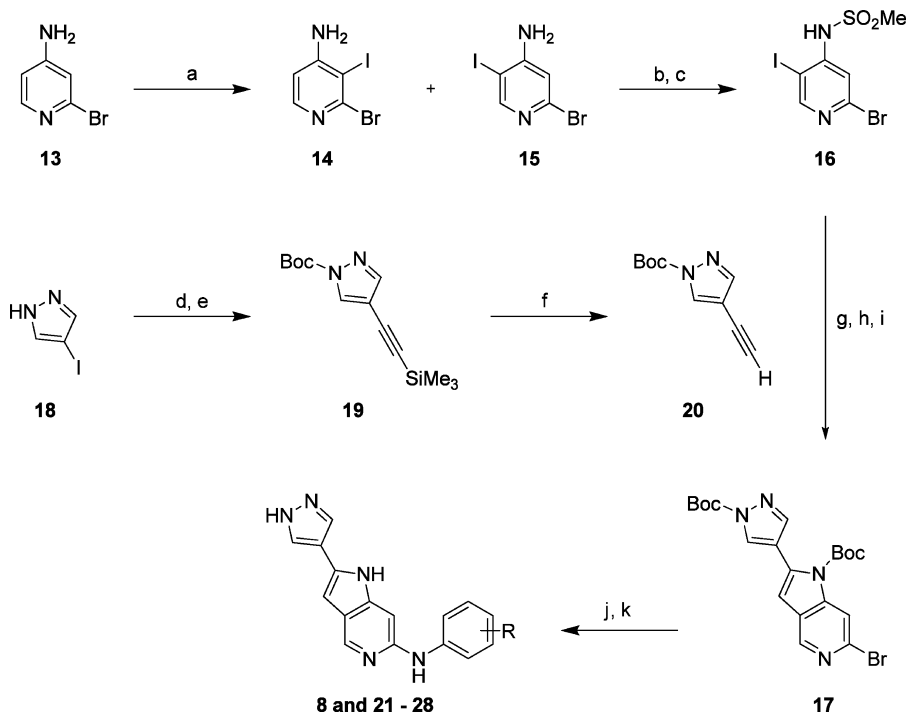
MPS1 IC₅₀ = 0.025±0.012 μM
CDK2 IC₅₀ = 0.043±0.023 μM
Aurora A IC₅₀ = 2.60 μM
Aurora B: 61% inhibition at 1 μM
GSK3β: 90% inhibition at 1 μM
MLM > 99% turnover (30 mins)
HLM = 49% turnover (30 mins)
Caco-2 efflux ratio >25

Figure 2. MPS1 inhibitor 8 identified by HTS (GSK3β, glycogen synthase kinase 3β; MLM, mouse liver microsome preparation; and HLM, human liver microsome preparation).

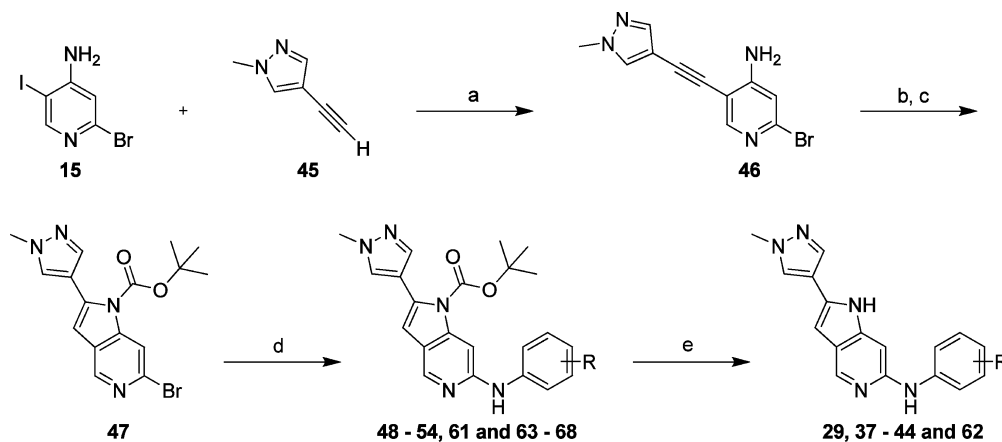
and an alkyne, 10, to generate key pyrrolopyridine intermediate 11, a domino approach recently exemplified by Schmidt and colleagues.²⁸ Subsequent palladium-mediated displacement of the 6-bromo substituent of intermediates 11 with the appropriate aniline gave the desired products 12 (Scheme 1). This general route was adapted depending on the identity of the N-1 and C-2 substituents as described below. We consistently observed that when R₁ = H the transformation of 11 to 12 was low-yielding; therefore, we employed a protecting-group strategy whereby a Boc substituent was installed at the N-1 position prior to introduction of the C-6 amino substituent into the 1*H*-pyrrolo[3,2-*c*]pyridine scaffold.

Compounds 8 and 21–28 shown in Table 1 were prepared according to the general strategy depicted in Scheme 1 using palladium-mediated substitution of key 6-bromo-pyrrolopyridine intermediate 17, which was itself prepared by sequential Sonagashira cross coupling and base-catalyzed ring closure of sulfonamide 16; introduction of the sulfonamide was necessary to optimize the efficiency of the domino cyclization reaction, presumably by increasing the acidity of the remaining anilinic proton (Scheme 2). Cyclization precursor 16 was prepared from corresponding 4-amino-2-bromopyridine 13; iodination of 13 was unselective, and desired regioisomer 15 was purified from its partner, 14, by chromatographic separation in 38 and 37% yields, respectively; subsequent dimesylation with methanesulfonylchloride and base-mediated removal of one of the two mesyl groups provided intermediate 16 in 54% yield. The required *tert*-butyl 4-ethynyl-1*H*-pyrazole-1-carboxylate 20 was prepared

Scheme 1. General Synthetic Strategy

Scheme 2. Preparation of 2-(1*H*-Pyrazol-4-yl)-1*H*-pyrrolo[3,2-*c*]pyridines^a

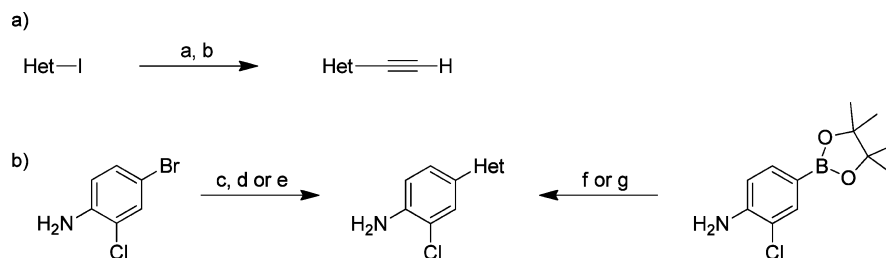
^aReagents and conditions: (a) ICl, NaOAc, AcOH, 75 °C; (b) MeSO₂Cl, Et₃N, CH₂Cl₂, rt; (c) NaOH, THF/H₂O, rt; (d) (Boc)₂O, Et₃N, THF, rt; (e) trimethylsilylacetylene, Pd(OAc)₂, PPh₃, CuI, *i*-Pr₂NH, DMF, 60 °C; (f) TBAF, THF, 0–5 °C; (g) PdCl₂(PPh₃)₂, CuI, Et₃N, DMF, 60 °C; (h) DBU, THF/MeOH, 40 °C; (i) (Boc)₂O, Et₃N, DMAP, EtOAc, rt; (j) aniline, Pd₂(dba)₃, Xantphos, Cs₂CO₃, dioxane, 80 °C; (k) TFA, CH₂Cl₂, rt.

Scheme 3. Preparation of Preferred *tert*-Butyl 2-(1-Methyl-1*H*-pyrazol-4-yl)-1*H*-pyrrolo[3,2-*c*]pyridine-1-carboxylates and 2-(1-Methyl-1*H*-pyrazol-4-yl)-1*H*-pyrrolo[3,2-*c*]pyridines^a

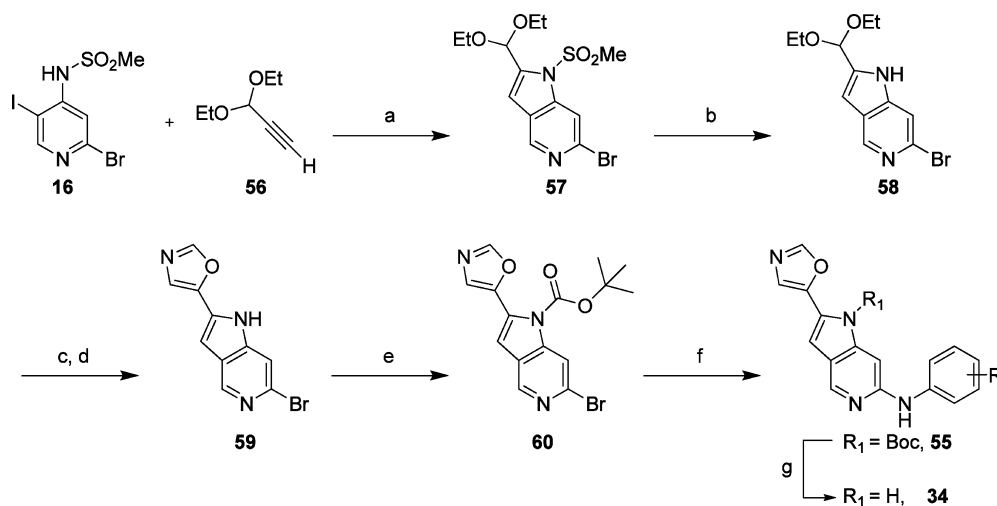
^aReagents and conditions: (a) PdCl₂(PPh₃)₂, CuI, Et₃N, DMF, rt; (b) *t*-BuOK, NMP, 50 °C; (c) (Boc)₂O, Et₃N, DMAP, EtOAc, rt; (d) aniline, Pd₂(dba)₃, Xantphos, Cs₂CO₃, DMA, 80 °C; (e) TFA, rt or TFA, CH₂Cl₂, rt.

in 56% overall yield from 4-iodopyrazole **18** by Boc protection followed by Sonogashira-mediated coupling with trimethylsilylacetylene and subsequent TBAF-mediated deprotection of alkyne **19** (Scheme 2).

Compounds **30–33**, **35**, and **36** in Table 2 were also prepared according to the general procedure (Scheme 1), which necessitated multiple protection/deprotection steps in addition to the need for bespoke synthesis of the appropriate

Scheme 4. Preparation of Alkyne and Aniline Intermediates^a

^aReagents and conditions: (a) trimethylsilylacetylene Pd(OAc)₂, PPh₃, CuI, *i*-Pr₂NH, DMF, 60 °C; (b) K₂CO₃, MeOH, rt, or TBAF, THF, 0–5 °C; (c) PdCl₂(dppf)·CH₂Cl₂, 1-methyl-4-(4,4,5,5-tetramethyl-1,3,2-dioxaborolan-2-yl)-1H-pyrazole, Na₂CO₃, THF/H₂O, reflux; (d) Pd(PPh₃)₄, pyridin-3-ylboronic acid, CsF, DME/MeOH, microwave, 150 °C; (e) Pd(OAc)₂, oxazole, di(1-adamantyl)-*n*-butylphosphine, pivalic acid, K₂CO₃, DMA, 110 °C; (f) Pd(PPh₃)₄, 3-iodo-1-methyl-1H-pyrazole or 5-iodo-1-methyl-1H-imidazole, Na₂CO₃, DME/H₂O, microwave, 135 °C; (g) PdCl₂(dppf)·CH₂Cl₂, 5-bromopyrimidine or 2-bromopyrazine, Na₂CO₃, DME, microwave, 75–150 °C.

Scheme 5. Preparation of 1H-Pyrrolo[3,2-*c*]pyridin-2-yl)oxazoles^a

^aReagents and conditions: (a) PdCl₂(PPh₃)₂, CuI, Et₃N, DMF, 60 °C; (b) NaOH, THF/H₂O, rt; (c) TsOH·H₂O, THF/H₂O, 25 °C; (d) TOSMIC, K₂CO₃, MeOH, 110 °C; (e) (Boc)₂O, Et₃N, DMAP, EtOAc, 25 °C; (f) aniline, Pd₂(dba)₃, Xantphos, Cs₂CO₃, dioxane or DMA, 80 °C; (g) TFA, CH₂Cl₂, rt.

ethynylheterocycle (see the Supporting Information). For compounds **29** and **37–44** (Table 2), **48–54** (Table 5), and **61–68** (Table 6) bearing a preferred 1-methylpyrazole substituent at C-2 of the pyrrolopyridine scaffold, we developed a more efficient route. Thus, Sonagashira cross coupling of 4-ethynyl-1-methyl-1H-pyrazole **45** with unprotected 4-amino-2-bromo-5-iodopyridine **15** gave cyclization precursor **46** in 88% yield, which was subjected to smooth base-mediated conversion to the pyrrolopyridine core followed by substitution of the N-1 position with a *tert*-butylcarbonate group to give key intermediate **47** in 75% yield (Scheme 3). This two-step, base-mediated approach to the formation of the pyrrolopyridine scaffold obviated the need for sulfonamide-mediated activation of the anilinic cyclization precursor. Subsequent palladium-mediated substitution at the C-6 position, as described above, gave N-1-Boc derivatives **48–54** (Table 5), **61**, and **63–68** (Table 6). TFA-mediated removal of the N-Boc substituent furnished N-1-unsubstituted compounds **29**, **37–44** (Table 2), and **62** (Table 6), as depicted in Scheme 3.

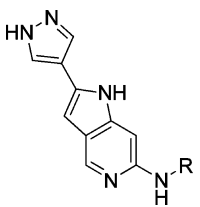
The required alkynes and substituted anilines were prepared according to the methods summarized in Scheme 4 (Supporting Information), whereas the appropriate iodoheterocycles were prepared from commercially available starting materials by iodination (Supporting Information). However,

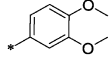
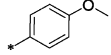
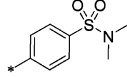
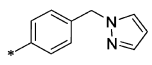
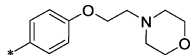
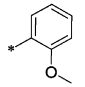
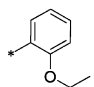
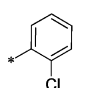
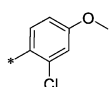
the 5-iodooxazole required for the synthesis of 1H-pyrrolo[3,2-*c*]pyridin-2-yl)oxazoles **34** and **55** proved elusive, and an alternative synthetic route was developed in which desired oxazole intermediate **60** was constructed from acetal **58** in 70% overall yield by liberation of the aldehyde and reaction with *p*-toluenesulfonylmethyl isocyanide (TOSMIC) followed by subsequent N-1 Boc protection. Acetal **58** was obtained from intermediate **16** in 45% yield by Sonogashira cross coupling with 3,3-diethoxyprop-1-yne **56** and concomitant ring closure in a procedure similar to that described by Le Brazidec et al. for the preparation of 2-substituted pyrrolopyrimidines followed by base-mediated removal of the N-1 sulfonamide (Scheme 5).²⁹

RESULTS AND DISCUSSION

Compound **8** (Figure 2) exemplifies a series of 1H-pyrrolo[3,2-*c*]pyridines discovered by HTS of an in-house kinase-focused compound library versus MPS1. Although compound **8** demonstrated potent, ligand-efficient³⁰ binding to MPS1 (IC₅₀ = 0.025 μM, LE = 0.43; Table 1) with evidence for cell-based antiproliferative activity in the HCT116 human colon cancer cell line (MTT assay, GI₅₀ = 0.55 μM), its overall profile suffered from poor selectivity, particularly against CDK2 (IC₅₀ = 0.043 μM), poor in vitro metabolic stability in mouse and human liver

Table 1. Effect of Aniline Substituents on MPS1 Selectivity



Compd	R	Biochemical IC ₅₀ (μM) or % inhibition at 1 μM				
		MPS1	CDK2	Aurora A	Aurora B	GSK3β
8		0.025±0.012	0.043±0.023	2.60 ^a	61%	90%
21		0.051±0.028	0.039 ^a	1.80±1.40	22%	73%
22		0.016±0.001	0.005±0.001	3.20±1.10	1.70 ^a	92%
23		0.021±0.012	0.026±0.017	4.2±3.3	2.3 ^a	90%
24		0.063±0.046	0.23±0.03	8.10±3.80	4.5 ^a	57%
25		0.025±0.011	0.97±0.08	28.00±21.00	> 100	13%
26		0.058±0.027	8.90±5.20	8.50±5.50	> 100	61%
27		0.028±0.021	0.80±0.60	49.00±29.00	> 100	56%
28		0.020±0.011	1.30±0.60	21.00±13.00	> 100	16%

microsomes, and significant efflux in Caco-2 permeability assays (Figure 2). An important aim of our initial hit-improvement strategy was to eradicate activity versus cell cycle kinases (e.g., CDK2) and other kinases known to affect mitotic function (e.g., Aurora kinases A and B) to study the profile of a highly selective MPS1 inhibitor on mitotic function in cellular mechanistic assays and in vivo. In addition, we set out to improve the metabolic stability and membrane permeability of compound 8 to discover a chemical tool suitable for in vivo PK/PD studies.

A crystal structure of the kinase domain of MPS1 with compound 8 (Figure 3) indicated binding of 8, albeit with relatively weak electron density. Nevertheless, the ligand could be modeled with partial occupancy along with a molecule of poly(ethylene glycol) wrapped around the active-site Lys553 side chain, a consequence of the presence of a high concentration of PEG300 in the crystallization conditions. The structure revealed the 6-amino-pyrrolopyridine motif interacting with the hinge region of the ATP-binding site by virtue of an H-bond-donor interaction between the backbone amide group of Gly605 and the pyridine nitrogen hydrogen-bond acceptor of the pyrrolopyridine scaffold. In addition, the anilinic NH of compound 8 formed a hydrogen bond with the carbonyl group of hinge residue Gly605, thereby positioning the anilinic moiety at the entrance of the MPS1 ATP-binding

site, stacked above the post-hinge region (residues 606–611) and pointing toward the solvent. Furthermore, it revealed an H-bond between the C-2 pyrazole and Lys553 as well as a van der Waals interaction between lipophilic C-3 to C-4 atoms and the gatekeeper residue, Met602 (Figure 3).

A striking difference between the binding of compound 8 and published compound 6 is their respective hydrogen-bond interactions with the hinge. Whereas the backbone functionalities of hinge residue Cys604 were not involved in interactions with compound 8, a peptide flip of Cys604 in the structure of MPS1 complexed with compound 6 (PDB code 3VQU) allowed an H-bond interaction between the backbone carbonyl of Cys604 and the anilinic NH of compound 6.²⁶

We initially focused our attention on modification of the pyrrolopyridine 6-anilino substituent to replace the electron-rich 3,4-dimethoxy aniline, which we regarded as a metabolic liability. 4-Methoxy analogue 21 proved equipotent and replacement with a range of 4-substituents maintained activity (compounds 22–24), consistent with the crystal structure of 8 bound to MPS1, which showed that this vector projects out of the entrance of the ATP-binding site into the solvent (Figure 3). However, selectivity versus CDK2 remained poor in all of these compounds. Importantly, the 2-methoxy-, 2-ethoxy-, and 2-chloro-substituted aniline derivatives, 25–28, maintained

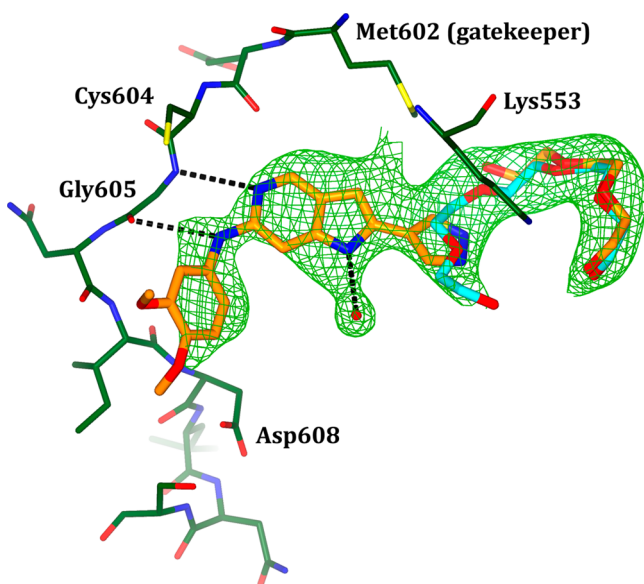


Figure 3. Crystal structure of MPS1 with compound **8** bound. Compound **8** is shown with orange carbon atoms and is modeled with partial occupancy along with a PEG molecule, shown with orange and cyan carbon atoms for the two alternate conformers. Selected amino acids that contact the ligand are shown with green carbon atoms. The electron density shown in green is from an $F_o - F_c$ omit map and is contoured at 3σ . Key H-bond interactions are shown as black dotted lines. The interaction between the C-2 pyrazole and Lys553 has been omitted for clarity. All structural figures were produced with CCP4MG.³¹

potency while also significantly improving selectivity versus CDK2 and enhancing selectivity versus Aurora A, Aurora B, and GSK3 β . This SAR is consistent with previous reports on the use of 2-substituted anilines in other chemical series to enhance selectivity versus MPS1 through the exploitation of a small lipophilic pocket adjacent to Cys604 in the hinge region (see below).²⁵

Compounds **25**–**28**, although selective for MPS1, remained metabolically unstable, and our attention turned to exploration of the pyrrolopyridine C-2 substituent. This was prompted by our observation that solutions of compound **8** underwent slow air oxidation across the double bond between C-2 and C-3 (Supporting Information Figure S1). We hypothesized that the unsubstituted C-2 pyrazole rendered the pyrrole moiety of the pyrrolopyridine scaffold susceptible to electrophilic attack. Gratifyingly, N-methylation of the C-2 pyrazole was tolerated with only a 5-fold reduction in potency (compound **29**, MPS1 IC_{50} = 0.12 μ M, versus compound **25**, MPS1 IC_{50} = 0.025 μ M; Table 2), resulting in an air-stable compound and a slight improvement in metabolic stability (MLM = 72% for **29** versus 99% for **25**) (Table 2). Similarly, electron-withdrawing trifluoroethyl-substituted pyrazole analogue **30** maintained potency (MPS1 IC_{50} = 0.079 μ M) and also improved metabolic stability (53% turnover in MLM); however, corresponding difluoromethyl analogue **31** proved surprisingly weak, with a 6-fold loss of activity with respect to the trifluoroethyl analogue (IC_{50} = 0.46 μ M for **31** versus 0.079 μ M for **30**). 1,3- and 1,5-Disubstituted pyrazole analogues (**32** and **33**) and the 3,5-disubstituted isoxazole **35** also lost potency despite an improvement in metabolic stability; we rationalized this loss of potency in terms of the sterically encumbered pocket into which the C-2-pyrazole substituent projects. Imidazole analogue **36** also lost potency in comparison with pyrazole

25 despite the presence of a potentially isosteric H-bond-donor or -acceptor interaction with Lys553, depending on the protonation state of the imidazole. Taken together, these results suggested tight SAR along the C-2 vector from the pyrrolopyridine scaffold and were consistent with the crystal structure of MPS1 complexed with compound **8** that showed that the interaction with Lys553 is important (Figure 3). Unsubstituted oxazole **34** proved to be the only potential C-2 pyrazole replacement that maintained potency with enhanced metabolic stability. The crystal structure of MPS1 in complex with oxazole **34** showed unambiguous electron density for the ligand, supporting the initial binding mode for compound **8** and consistent with the SAR observed for the aniline and C-2 heterocycle modifications made to the pyrrolopyridine scaffold (Figure 4). The hinge-binding motif was the same as that

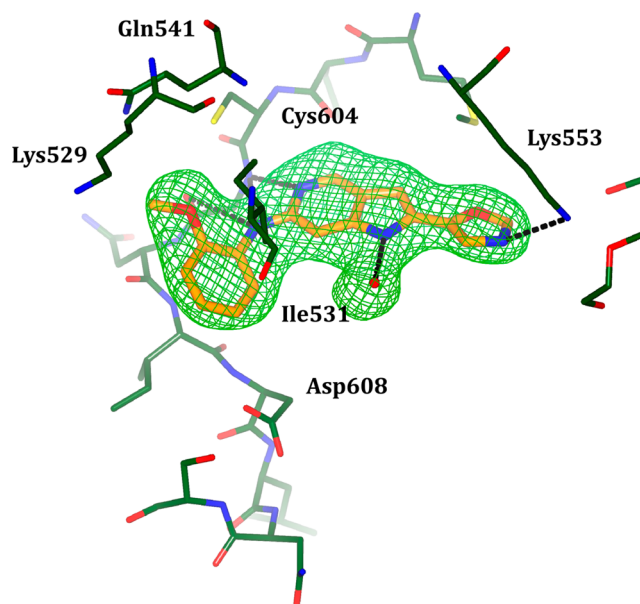


Figure 4. Crystal structure of MPS1 with compound **34** bound. Compound **34** is shown with orange carbon atoms. Selected amino acids that contact the ligand are shown with dark green carbon atoms. H-bond interactions are shown as black dotted lines. The electron density shown in green is from an $F_o - F_c$ omit map and is contoured at 3σ .

observed with compound **8**, and the aniline C-2-methoxy substituent was positioned, as expected, in a small hydrophobic pocket lined by Lys529, Ile531, Gln541, and the gatekeeper +2 residue, Cys604. This pocket is not accessible in many other kinases, including CDK2, GSK3 β , Aurora A, and Aurora B, which have bulkier residues at the corresponding gatekeeper +2 position (Phe in CDK2 and Tyr in GSK3 β and Aurora A and B). This is consistent with improved selectivity for MPS1 versus related kinases observed for compounds with an aniline 2-substituent (Tables 1 and 2).²⁵ Like the pyrazole of compound **8**, the oxazole of **34** was oriented toward the catalytic Lys553 residue, and an H-bond was observed between the pyrrolopyridine N-1 atom and a water molecule. However, despite the presence of a preferred aniline C-2-substituent, the weak CDK2 activity of **34** coupled with the relative complexity of the synthetic route to C-2 oxazoles (Scheme 5) disfavored this approach. We selected 1-methylpyrazole in preference to the 1-trifluoroethyl pyrazole as the optimal pyrrolopyridine C-2 substituent because of its lower lipophilicity and improved ligand efficiency.

Table 2. Effect of Pyrrolopyridine C-2 and Aniline C-4 Substituents on Metabolism

The image shows the chemical structure of a pyrrolopyridine derivative. It consists of a fused pyrrole and pyridine ring system. The pyrrole ring has an NH group and a substituent R¹ at the 2-position. The pyridine ring has a substituent R² at the 4-position.

Compd	R ¹	R ²	Biochemical IC ₅₀ (μM)				MLM ^a
			MPS1	CDK2	Aurora A	Aurora B	
25			0.025±0.011	0.97±0.08	28.00±21.00	> 100	99%
29			0.12±0.08	53.00±38.00	> 100	> 100	72%
30			0.079±0.029	> 100	> 100	> 100	53%
31			0.46±0.03	> 100	> 40	> 100	61%
32			0.99±0.41	> 100	> 100	> 100	30%
33			1.60±0.27	> 100	> 100	> 100	97%
34			0.026±0.010	2.90±0.57	> 40	> 100	11%
35			4.90±2.10	> 100	> 100	16.00 ^b	38%
36			0.64±0.08	7.80±0.62	72.00±29.00	47.00 ^b	87%
37			4.40±0.34	> 100	> 100	> 100	56%
38			0.074±0.005	46.00±7.40	> 100	> 100	41%
39			0.015±0.004	7.80±1.60	> 40	> 100	25%

Table 2. continued

Compd	R ¹	R ²	Biochemical IC ₅₀ (μM)				MLM ^a
			MPS1	CDK2	Aurora A	Aurora B	
40			0.023±0.001	43.00±7.20	> 100	> 100	21%
41			0.027±0.009	7.90±3.20	> 100	> 100	20%
42			0.013±0.001	9.40±5.50	> 100	> 100	23%
43			0.020±0.001	5.20±0.90	> 100	34.00±20.00	15%
44			0.008±0.003	4.20±1.00	> 100	> 100	4.5%

^aMLM: percentage of parent compound metabolized after a 30 min incubation in mouse liver microsomes. ^b*n* = 1.

We then investigated a range of aniline substitutions with the aim of further improving metabolic stability by reduction of both lipophilicity and electron density in the aniline moiety. 2-Methoxy-5-trifluoromethyl analogue **37** (IC₅₀ = 4.4 μM; Table 2) illustrates poor tolerance of a 2,5-disubstitution pattern on the aniline ring. Analysis of the compound **34**-bound MPS1 structure suggested that the addition of a CF₃ substituent to the 5-position of the aniline ring would induce a steric clash with Asp608 (Figure 4). This observation is consistent with the SAR described for a series of Leucine Rich Repeat Kinase 2 (LRRK2) inhibitors in which a 2,5-disubstituted aniline was employed to drive selectivity for LRRK2 over MPS1.³² Exploitation of the aniline C-4 vector, which extends into the solvent channel (Figure 3), was more successful and led to the synthesis of compounds **39–44**, all of which displayed good potency compared to their unsubstituted parent **38**, improved selectivity, and in vitro metabolic stability (Table 2). However, the measured aqueous thermodynamic solubility was low (e.g., 0.01 mg/mL for compound **42**).

2-Chloro-4-dimethylcarboxamido-substituted aniline **39** was selected for pharmacokinetic evaluation on the basis of its excellent potency, in vitro selectivity, and improved metabolic stability in mouse and human liver microsomes (25 and 20% turnover after a 30 min incubation, respectively). This compound displayed an improved efflux ratio in Caco-2 (10) compared to original hit compound **8** and demonstrated good in vivo pharmacokinetics in mouse with a low unbound clearance and moderate oral bioavailability, consistent with our strategy of targeting improved in vitro metabolic stability versus compound **8** (Table 3).

A crystal structure of compound **39** bound to MPS1 was obtained by soaking MPS1 crystals for 24 h in a solution

containing 1.25 mM of the inhibitor. The crystal structure showed that the overall binding mode of **39** was very similar to those of HTS hit compound **8** and oxazole **34**. However, the crystallographic data revealed significant electron density along a vector aligned from the pyrrolopyridine N-1 position (Figure 5A), which could not be explained by the interacting water molecule observed in the compound **8**-bound and compound **34**-bound structures. Analysis of the compound sample used for the soaking experiment revealed a 2% impurity of the N-Boc synthetic precursor (**48**; Table 5), which fitted well with the additional electron density observed in the crystal structure. We reasoned that to preferentially occupy the ATP-binding site in a soaking experiment involving a 50-fold excess of compound **39**, compound **48** must be significantly more potent than compound **39**. Subsequent elucidation of the crystal structure of MPS1 bound to the N-Boc-containing precursor, compound **48**, confirmed this hypothesis because the overall binding mode of **48** was entirely consistent with the other crystal structures and the Boc group was clearly present in the same location as the additional electron density in the compound **39**-bound structure (Figure 5B). The aniline C-2-chloro substituent of compound **48** was located in the same lipophilic pocket as the aniline C-2-methoxy group in compound **34**, consistent with the improved selectivity afforded by small lipophilic substituents in the aniline C-2 position (Tables 1 and 2).

Compound **48** displayed potency at the low end of the dynamic range of our in vitro MPS1 assay (IC₅₀ = 0.006 μM; Table 5; MPS1 enzyme concentration = 3–12.5 nM, see the Supporting Information). We therefore set up a high-throughput cell-based assay that measures the inhibition of ectopic MPS1 autophosphorylation at Thr33 and Ser37 using

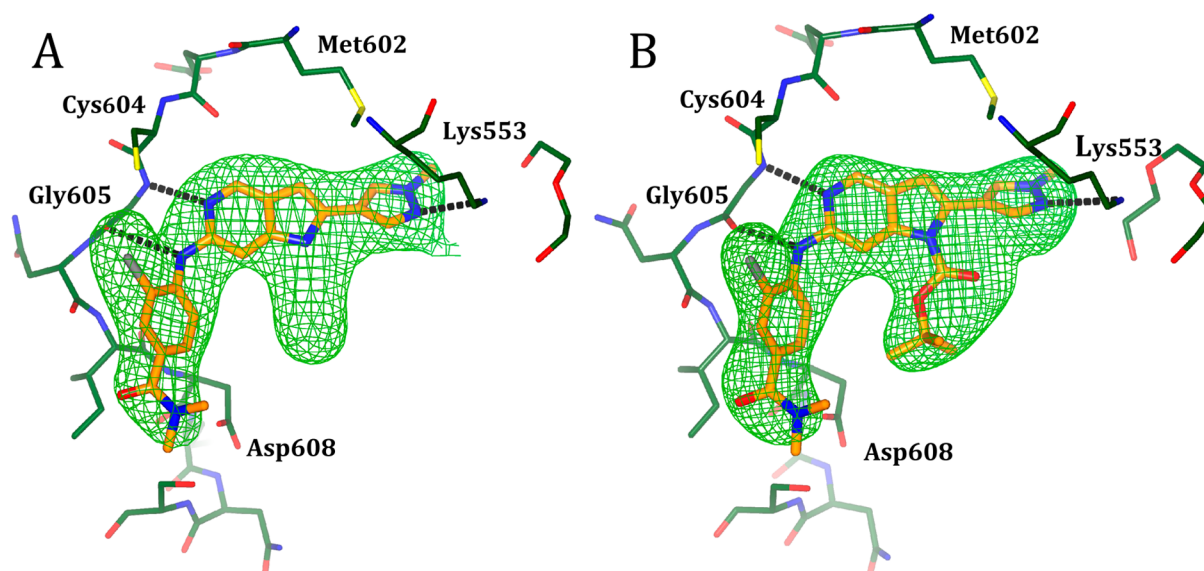


Figure 5. Crystal structure of MPS1 with compounds **39** (panel A) and **48** (panel B) bound. Compounds **39** and **48** are shown with orange carbon atoms. Selected amino acids that contact the ligands are shown with dark green carbon atoms. H-bond interactions are shown as black dotted lines. The electron density shown in green in each panel is from an $F_o - F_c$ omit map and is contoured at 3σ .

Table 3. In Vivo Mouse Plasma Pharmacokinetic Profile of **39** after Oral and iv Dosing (10 mg/kg)

$t_{1/2}$ (h)	Cl (mL/min/kg)	PPB (%)	Clu (mL/min/kg)	V_d (L/kg)	F (%)
1.05	4.74	94.1	80	0.32	48

Table 4. In Vivo Mouse Plasma Pharmacokinetic Profile of **48** after Oral and iv Dosing (5 mg/kg)

$t_{1/2}$ (h)	Cl (mL/min/kg)	PPB (%)	Clu (mL/min/kg)	V_d (L/kg)	F (%)
3.26	12.44	99.5	2589	1.99	78

an MSD electrochemiluminescent readout (see the Supporting Information) to discriminate more potent compounds. Comparison of compound **39** and its N-Boc precursor **48** in this assay revealed a 7-fold increase in cellular potency because of the N-Boc substituent (P-MPS1 $IC_{50} = 0.60 \mu\text{M}$ for compound **48** versus $4.10 \mu\text{M}$ for compound **39** and HCT116 $GI_{50} = 2.20 \mu\text{M}$ for compound **48** versus $9.80 \mu\text{M}$ for compound **39**; Table 5). We hypothesized that a combination of increased in vitro potency and lipophilicity-driven cell penetration was responsible for the increase in cellular potency. Gratifyingly, compound **48** not only retained metabolic stability in mouse and human liver microsomes (48 and 34% turnover after a 30 min incubation, respectively; Table 5) despite increased lipophilicity (**48** AlogP = 5.1, **39** AlogP = 3.0) but also displayed reasonable chemical stability in aqueous acid and base (38% cleavage of the Boc group was observed after a 75 min incubation of **48** in a simulated gastric acid fluid at 37°C , and no cleavage was observed after a 5 h incubation of **48** in a simulated duodenum solution at 37°C), indicating that the N-1-Boc substituent of compound **48** may survive gut media on oral administration. Moreover, the increased lipophilicity of **48** improved passive permeability (PAMPA $>100 \times 10^{-6} \text{ cm/s}$ at pH 7.4) and abrogated Caco-2 efflux (A to B = $17 \times 10^{-6} \text{ cm/s}$, efflux ratio = 1). In vivo pharmacokinetic profiling in mouse revealed increased clearance, consistent with higher lipophilicity and MLM metabolic turnover (48% for **48** at 30 min versus 25% for **39**), increased volume of distribution, and higher bioavailability compared to compound **39**, consistent with increased lipophilicity and passive permeability (Table 4).

Finally, we were concerned that increased lipophilicity imparted by our serendipitous discovery of the influential N-Boc substituent might erode the in vitro selectivity profile; however, selectivity versus CDK2 and Aurora A was maintained (Table 5), and we also observed complete selectivity over other mitotic kinases, for example, NIMA-related kinase 2 (NEK2) and Polo-Like Kinase 1 (PLK1) ($IC_{50} > 100 \mu\text{M}$). Thus, compound **48** resolved many of our issues with original hit compound **8**, and we elected to maintain the N-1-Boc substituent in further analogues. We next turned our attention to improvement of the cell-based GI_{50} in HCT116 cells, which remained relatively weak for compound **48** ($GI_{50} = 2.20 \mu\text{M}$; Table 5).

As expected, further exploration of the aniline C-4 vector in the N-Boc-substituted pyrrolopyridine series revealed broad tolerance for a variety of substituents, with optimal translation to cell-based potency observed for azetidine amide **51**, piperidine amides (**52** and **53**), and thiomorpholine 1,1-dioxide amide **54**. Consistent with previous SAR, we were pleased to note that C-2-oxazole **55** was also tolerated in this series (Table 5), and the crystal structure of **55** bound to MPS1 confirmed that the oxazole maintains an interaction with Lys553 (Figure 6), consistent with the structure of MPS1 with compound **34**. However, neither the C-2-oxazole nor the C-2-pyrazole compounds with variations at the aniline C-4 vector provided a significant improvement in cell-based antiproliferative activity (Table 5).

Analysis of the crystal structures of compounds **48** (Figure 5B) and **55** (Figure 6) showed that the aniline C-4 dimethylamido substituent projected toward the solvent above the Asp608–Ser611 helix-capping motif in the post-hinge region of the kinase.

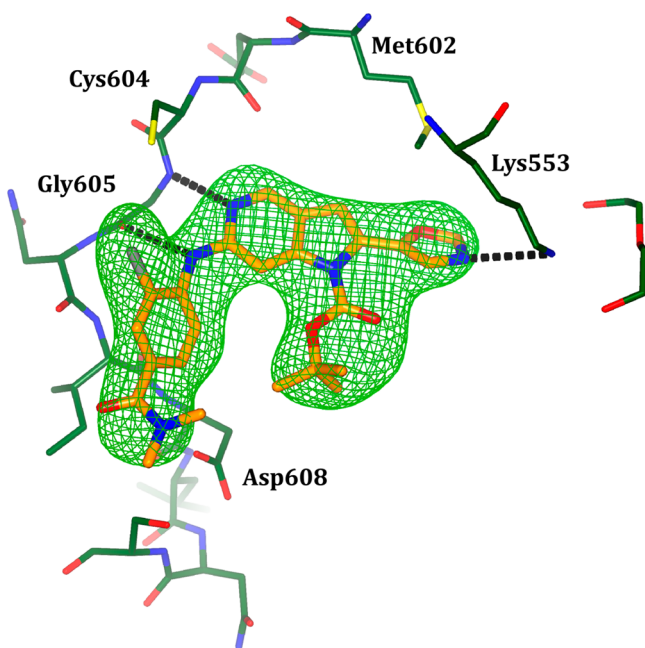


Figure 6. Crystal structure of MPS1 with compound 55 bound. Selected amino acids are shown with dark green carbon atoms. Compound 55 is shown with orange carbon atoms. H-bond interactions are shown as black dotted lines. The electron density shown in green is from an $F_o - F_c$ omit map and is contoured at 3σ .

This suggested that replacement of the aniline 4-amido substituent with an appropriate heterocycle may be tolerated, and we were keen to explore the effect of this modification on cellular potency (Table 6). Gratifyingly, C-4-pyrazolo analogues **61**, **62**, and **63** proved to be potent inhibitors of MPS1 in the in vitro biochemical assay, with acceptable metabolic stability in mouse and human liver microsomes. Analogous to our observations with compounds **39** and **48**, we observed a significant (43-fold) increase in inhibition of MPS1 autophosphorylation in cells for N-1-Boc-substituted compound **61** versus its N-1-H analogue **62** (P-MPS1 IC_{50} = $0.16 \mu\text{M}$ versus $6.90 \mu\text{M}$), and this improvement was also observed in an assay of cell proliferation (**61**, HCT116 GI_{50} = $0.50 \mu\text{M}$; **62**, HCT116 GI_{50} = $4.60 \mu\text{M}$). Although oxazole-substituted analogue **64** and those substituted with six-membered heterocycles, **66**–**68**, all maintained potent inhibition of MPS1 in vitro, translation to cell-based activity was not improved compared to pyrazole **61** (Table 6). However, the 1-methyl-imidazol-5-yl moiety at the 4-position of the aniline (compound **65**) conferred improved translation to cell-based potency (P-MPS1 IC_{50} = $0.04 \mu\text{M}$ and HCT116 GI_{50} = $0.16 \mu\text{M}$), which is comparable to or better than the cell-based potency of reported MPS1-selective inhibitors tested in our assays (Table 7).

Compound **65** displayed in vitro potency versus MPS1 at the low end of the dynamic range of our in vitro assay, which together with an excellent translation to cell-based assays prompted further analysis of the binding mode of **65** by X-ray crystallography (Figure 7A). The structure was determined by cocrystallization of the kinase domain of MPS1 with **65** using PEG3350 as the precipitant instead of PEG300 in an attempt to remove the artificial PEG molecule bound in the ATP-binding site. This resulted in a more physiologically relevant structure without a PEG molecule wrapped around the active-site Lys553 residue, which allowed for the formation of the conserved Lys553–Glu571 ion-pair. Although the binding mode of compound **65** was entirely consistent with our previous compound-bound crystal structures,

MPS1 activation-loop residues Ala668–Thr675 adopt an ordered conformation, and the ordered loop forms an antiparallel β -sheet interaction with the P-loop (Figure 7B). In addition, activation-loop residues Met671–Pro673 form a complementary hydrophobic pocket wrapped around the N-1-Boc substituent of **65**, completely enclosing the inhibitor in the ATP-binding site. Intriguingly, this activation-loop conformation has previously been observed in the crystal structure of MPS1 with a pyrimidodiazepine ligand (PDB code 3H9F)²⁰ and is incompatible with binding of a PEG molecule around Lys553 because of steric hindrance. In this structure, a triply phosphorylated Thr–Thr–Ser motif at residues 675–677 formed magnesium-mediated crystal contacts, which may have influenced the activation-loop conformation. A careful analysis of two recently reported crystal structures of MPS1, one in complex with a diamino-pyridine inhibitor (PDB code 3VQU)²⁶ and one with an early indazole-based inhibitor (PDB code 3W1F),²⁷ also showed a similarly ordered activation loop in both structures but with the Thr–Thr–Ser motif disordered. In our compound **65**-bound MPS1 structure, Thr676 and Ser677 are also disordered, and we did not observe electron density for a phosphate group on Thr675 or for the mediating magnesium atoms. This suggests that in our **65**-bound MPS1 structure these residues are not involved in meaningful crystal contacts that could have an effect on the conformation of the activation loop. Further analysis of the crystal packing showed that the only residue of a symmetry-related molecule that is in the vicinity of the activation loop is Ile738. However, a comparison of several compound-bound structures (Supporting Information Figure S2A) showed that Ile738 is located in a region of the protein with only minor conformational flexibility, whereas the activation loop in the respective structures shows a wide range of conformations and a varying degree of order. The absence of any concerted conformational changes between the activation loop and the symmetry-related Ile738 region in these structures led us to conclude that the ordering of the activation loop is not influenced by crystal contacts. Nevertheless, the ordering of the activation loop is clearly prevented by the binding of a PEG molecule in MPS1 structures resulting from the PEG300-containing crystallization conditions. This is supported by soaking MPS1 crystals grown in PEG300 with compound **65**, which resulted in a **65**-bound MPS1 structure with a disordered activation loop (data not shown).

The structures of MPS1 in complex with the precursors of the diamino-pyridine and indazole-based inhibitors **6**²⁶ and **7**²⁷ show an ordering of the activation loop through interactions with the P-loop and an ethoxy-group, which in both inhibitors is located in a similar position as the N-1-Boc substituent in **65**. Moreover, in the pyrimidodiazepine-bound MPS1 structure, the inhibitor interacts with the ordered activation loop via a cyclopentyl moiety in a similar position as the N-1 Boc in compound **65**. Taken together, these findings support the hypothesis that the ordering of the activation loop might have a compound-dependent component for inhibitors with substituents similar to the N-1 Boc in compound **65**.

It is important to note that the overall structure of the MPS1 kinase domain in the compound **65**-bound structure has many features of an active kinase conformation. These include the positioning of the αC -helix and the conserved DFG motif in an “in” conformation as well as the presence of the canonical active Lys553–Glu571 ion pair. Further analysis of the conformation in light of the “spine concept”³³ clearly shows the presence of the catalytic C-spine and shows only minor distortions in the regulatory R-spine (Supporting Figure 2B), also indicating that the conformation of MPS1 in this structure

Table 5. Effect of the N-1-Boc Substituent on Cell-Based Potency

Compd	R ¹	R ²	R ³	Biochemical IC ₅₀ (μM)			Cellular activity (μM)		MLM ^a	HLM ^a
				MPS1	CDK2	Aurora A	P-MPS1 IC ₅₀	HCT116 GI ₅₀		
39		H		0.015±0.004	7.80±1.60	> 40	4.10±2.60	9.80±1.90	25%	20%
48		Boc		0.006±0.003	1.90±0.22	23.00±10.00	0.60±0.49	2.20±0.13	48%	34%
49		Boc	H	0.071±0.012	> 100	> 100	3.40±1.90	4.20±0.52	ND	ND
50		Boc		0.092±0.046	> 100	> 100	0.84±0.68	1.65±0.11	66%	81%
51		Boc		0.007±0.001	5.50±0.75	> 100	0.23±0.15	1.40±0.68	40%	51%
52		Boc		0.011±0.004	2.80±0.99	65.00±5.10	0.72±0.56	3.00±1.00	ND	ND
53		Boc		0.004±0.001	0.68±0.15	17.00±3.90	1.10±1.10	2.00±1.40	56%	96%
54		Boc		0.005±0.001	0.75±0.05	53.00±6.00	0.86±0.59	4.90±1.30	12%	23%
55		Boc		0.022±0.001	0.16±0.05	75.00±6.40	5.60 ^c	4.2 ^c	58%	ND

^aMLM/HLM: percentage of parent compound metabolized after a 30 min incubation. ^bND = not determined. ^c*n* = 1.

is close to an active kinase conformation. However, the compound-induced conformation of the activation loop is incompatible with ATP binding and substrate-peptide binding to the kinase because it blocks the phosphate-binding region and the peptide binding site is not formed, a situation that would certainly render MPS1 inactive (Figure 7D).

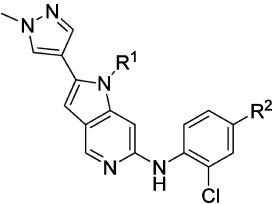
Introduction of the methylimidazole into compound **65** resulted in compromised passive permeability (PAMPA = 18×10^{-6} cm/s at pH 7.4) and increased efflux (Caco-2 A to B = 5×10^{-6} cm/s, B to A = 12×10^{-6} cm/s, ER = 2.5) compared to compound **48**. Although the thermodynamic aqueous solubility of compound **65** was very low (<0.001 mg/mL), solubility in fasted- and fed-state-simulated intestinal fluid (FaSSIF and FeSSIF) was 0.01 and ~0.55 mg/mL, respectively, consistent with the presence of a weakly basic center (the methylimidazole ring). All other in vitro properties were maintained, and in view of its favorable in vitro profile, compound **65** was selected for more extensive in vitro profiling versus a panel of 121 kinases (Supporting Information Table S1) and in vivo pharmacokinetic evaluation. Of the 121 kinases in the panel, MPS1 showed the greatest inhibition by **65**,

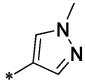
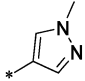
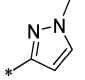
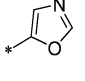
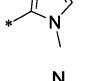
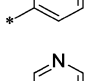
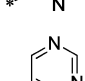
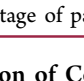
and only three other kinases showed inhibition greater than 80%. Mouse and rat blood pharmacokinetics revealed a favorable profile with moderate clearance and good to moderate oral bioavailability (Table 8). This compound was progressed to a human tumor xenograft model to test whether pharmacodynamic biomarker modulation could be achieved in vivo. Oral administration of two doses of compound **65** at 50, 75, and 100 mg/kg b.i.d. to mice bearing HCT116 human colon carcinoma xenografts demonstrated dose-dependent modulation of MPS1-driven phospho-histone H3 levels versus control animals at 2 and 10 h but not at 72 h after the last dose, consistent with engagement of MPS1 in vivo (Figure 8A). The compound was well-tolerated at all doses, and the observed decrease in phospho-histone H3 inhibition over time by compound **65** tracks with a decrease in total plasma and tumor tissue exposure measured in the same experiment (Figure 8B,C).

CONCLUSIONS

We describe the structure-based optimization of a potent but nonselective and metabolically unstable 1H-pyrrolo[3,2-c]-pyridine HTS hit **8** to compound **65**, a highly potent inhibitor

Table 6. Effect of the Aniline Substituent on Cell-Based Potency



Compd	R ¹	R ²	Biochemical IC ₅₀ (μM)			Cellular activity (μM)		MLM ^a	HLM ^a
			MPS1	CDK2	Aurora A	P-MPS1 IC ₅₀	HCT116 GI ₅₀		
61	Boc		0.015±0.013	> 100	> 100	0.16±0.12	0.50±0.15	29%	24%
62	H		0.017±0.001	> 100	> 100	6.90±5.80	4.60±0.67	49%	33%
63	Boc		0.020±0.002	> 100	> 100	2.50±0.42	4.40±0.11	35%	20%
64	Boc		0.019±0.009	>40	> 100	0.26±0.02	0.97±0.72	23%	20%
65	Boc		0.003±0.002	> 100	> 40	0.043±0.026	0.16±0.09	28%	51%
66	Boc		0.028±0.018	> 100	> 100	0.71±0.64	1.30±0.96	13%	43%
67	Boc		0.032±0.006	> 100	> 100	0.62±0.54	1.30±0.55	26%	25%
68	Boc		0.021±0.017	> 50	> 50	0.21 ^b	0.53 ^b	12%	16%

^aMLM/HLM: percentage of parent compound metabolized after a 30 min incubation in mouse and human liver microsomes. ^b_n = 1.

Table 7. Comparison of Compound 65 (CCT251455) with Reported MPS1 Inhibitors

compd	biochemical IC ₅₀ (μM)			cellular activity (μM)	
	MPS1	CDK2	Aurora A	P-MPS1 IC ₅₀	HCT116 GI ₅₀
65	0.003 ± 0.002	>100	>40	0.043 ± 0.026	0.16 ± 0.09
4	0.007 ± 0.009	36.00 ^a	21.00 ± 11.00	0.72 ^a	1.20 ^a
5	0.007 ± 0.003	>100	>30	0.16 ± 0.12	0.18 ± 0.09
6	0.011 ± 0.004	8.80 ^a	>100	0.56 ± 0.24	1.60 ± 0.75

^a_n = 1.

of MPS1 that demonstrates high selectivity versus kinases tested in a broad kinome profiling panel. We observed excellent translation of in vitro biochemical potency versus isolated MPS1 enzyme to cell-based potency (P-MPS1 IC₅₀ = 0.04 μM and HCT116 GI₅₀ = 0.16 μM), which is comparable to or better than the cell-based potency of other literature-reported MPS1-selective inhibitors tested side-by-side in our assays. Medicinal-chemistry optimization to **65** was educated by structure-based design; in particular, incorporation of an N-1-carbamate substituent was inspired by our observation that the activation loop of MPS1 became ordered in the presence of this substituent. The crystal structure of **65** in MPS1 confirmed this activation-loop stabilization, which results in an occluded

ATP-binding site and is incompatible with ATP and substrate binding. Despite the increased lipophilicity imparted by the carbamate moiety, **65** demonstrates a good oral pharmacokinetic profile in mouse and rat as well as inhibition of MPS1 activity in vivo following oral administration; **65** is a suitable chemical probe³⁵ for cell-based assays and in vivo evaluation of the effect of MPS1 inhibition in human tumor xenograft models.

EXPERIMENTAL SECTION

Chemistry. Commercially available starting materials, reagents and dry solvents were used as supplied. Flash column chromatography was

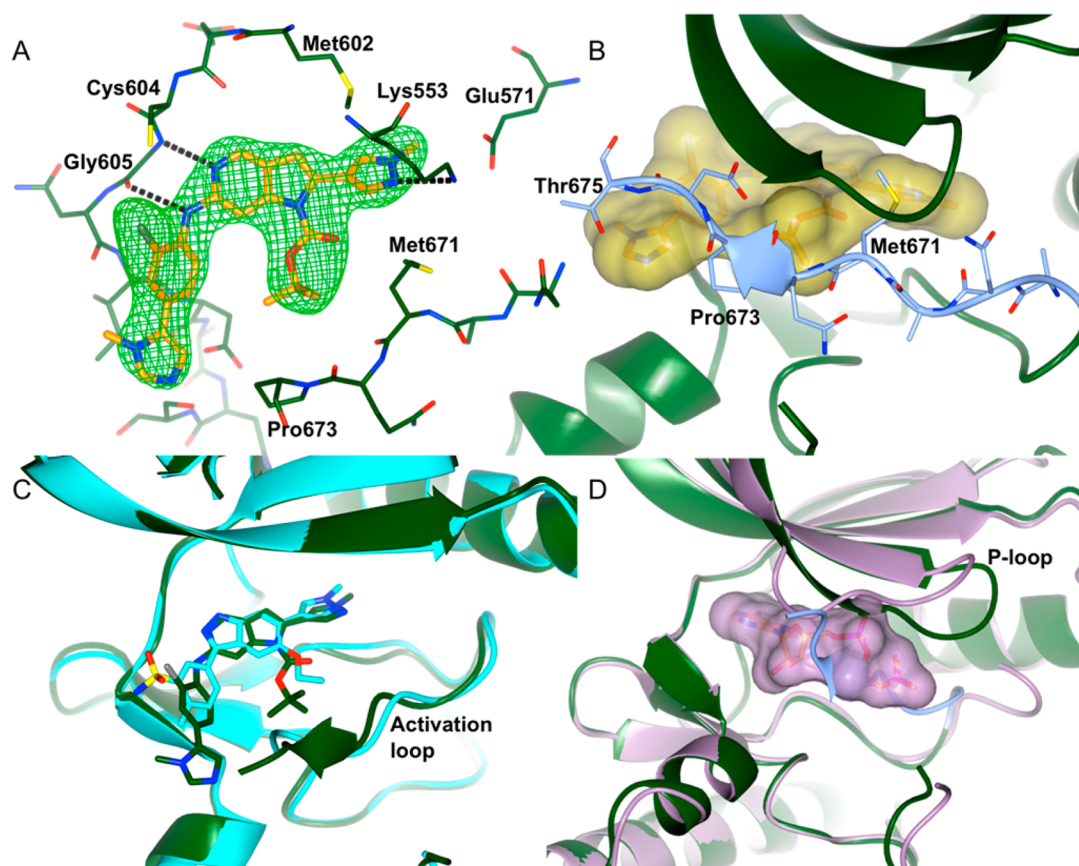


Figure 7. Crystal structure of MPS1 with compound **65** bound. (A) Selected amino acids are shown with dark green carbon atoms. Compound **65** is shown with orange carbon atoms. H-bond interactions are shown as black dotted lines. The electron density shown in green is from an $F_o - F_c$ omit map and is contoured at 3σ . (B) Compound **65** is shown as a surface, and MPS1 is shown in dark green as ribbons. Activation-loop residues Ala668–Thr675 are highlighted with blue carbon atoms and blue ribbon representation. (C) Superposition of the compound **65**-bound MPS1 structure in green and the structure of MPS1 complexed with an indazole-based inhibitor (PDB code 3W1F)²⁷ in cyan, with an ethoxy-group in similar position as the N-1 Boc in compound **65**. The ordered activation loops interacting with the respective inhibitors are indicated. (D) Comparison of the ATP-bound structure of MPS1 (PDB code 3HMN)³⁴ shown in lilac with the compound **65**-bound structure shown in green. The activation loop in the MPS1-**65** complex structure is highlighted in blue, and clashes with all three phosphates of ATP in the 3HMN structure.

Table 8. Mouse and Rat in Vivo PK Profile of Compound **65 Dosed at 5 mg/kg iv/po**

species	$t_{1/2}$ (h)	Cl (mL/min/kg)	PPB (%)	V_d (L/kg)	F (%)
mouse	4.2	23.8	99.93	2.3	83
rat	3.1	7.04	ND	1.75	32

ND = not determined.

performed using Merck silica gel 60 (0.025–0.04 mm). Column chromatography was also performed on a FlashMaster personal unit using isolate Flash silica columns or a Biotage SP1 purification system using Merck or Biotage Flash silica cartridges. Preparative TLC was performed on Analtech or Merck plates. Ion-exchange chromatography was performed using acidic Isolute Flash SCX-II columns, Isolute Si-carbonate columns, or basic Isolute Flash NH₂ columns. Preparative HPLC was conducted using a Phenomenex Luna column (5 μ m, 250 \times 21.2 mm, C18, Phenomenex, Torrance, USA) using a Gilson GX-281 liquid handler system combined with a Gilson 322 HPLC pump (Gilson, Middleton, USA) over a 15 min gradient elution from 10:90 to 100:0 MeOH/water (both modified with 0.1% formic acid) at a flow rate of 20 mL/min or over a 15 min gradient elution from 40:60 to 100:0 MeOH/water (both modified with 0.1% formic acid) at a flow rate of 20 mL/min. UV–vis spectra were acquired at 254 nm on a Gilson 156 UV–vis detector (Gilson, Middleton, USA). Collection was triggered by UV signal and collected using a Gilson GX-281 liquid handler system (Gilson, Middleton, USA). Raw data

was processed using Gilson Trilution Software. ¹H NMR spectra were recorded on a Bruker Avance-500. Samples were prepared as solutions in a deuterated solvent and referenced to the appropriate internal deuterated solvent peak or tetramethylsilane. Chemical shifts were recorded in ppm (δ) downfield of tetramethylsilane. LC/MS analysis was performed on a Waters Alliance 2795 Separations Module and Waters 2487 dual-wavelength absorbance detector coupled to a Waters/Micromass LCt time-of-flight mass spectrometer with ESI source. Analytical separation was carried out at 30 °C either on a Merck Chromolith SpeedROD column (RP-18e, 50 \times 4.6 mm) using a flow rate of 2 mL/min in a 3.5 min gradient elution with detection at 254 nm or on a Merck Purospher STAR column (RP-18e, 30 \times 4 mm) using a flow rate of 1.5 mL/min in a 3.5 min gradient elution with detection at 254 nm. The mobile phase was a mixture of MeOH (solvent A) and water (solvent B), both containing formic acid at 0.1%. Gradient elution was as follows: 1:9 (A/B) to 9:1 (A/B) over 2.25 min, 9:1 (A/B) for 0.75 min, and then reversion back to 1:9 (A/B) over 0.3 min, and finally 1:9 (A/B) for 0.2 min (also referred to as ESI-HRMS method A). LC/MS and HRMS analyses were performed on an Agilent 1200 series HPLC and diode array detector coupled to a 6210 time-of-flight mass spectrometer with dual multimode atmospheric pressure CI/ESI source. Analytical separation was carried out at 30 °C either on a Merck Chromolith SpeedROD column (RP-18e, 50 \times 4.6 mm) using a flow rate of 2 mL/min in a 4 min gradient elution with detection at 254 nm or on a Merck Purospher STAR column (RP-18e, 30 \times 4 mm) using a flow rate of 1.5 mL/min in a 4 min gradient elution with detection at 254 nm.

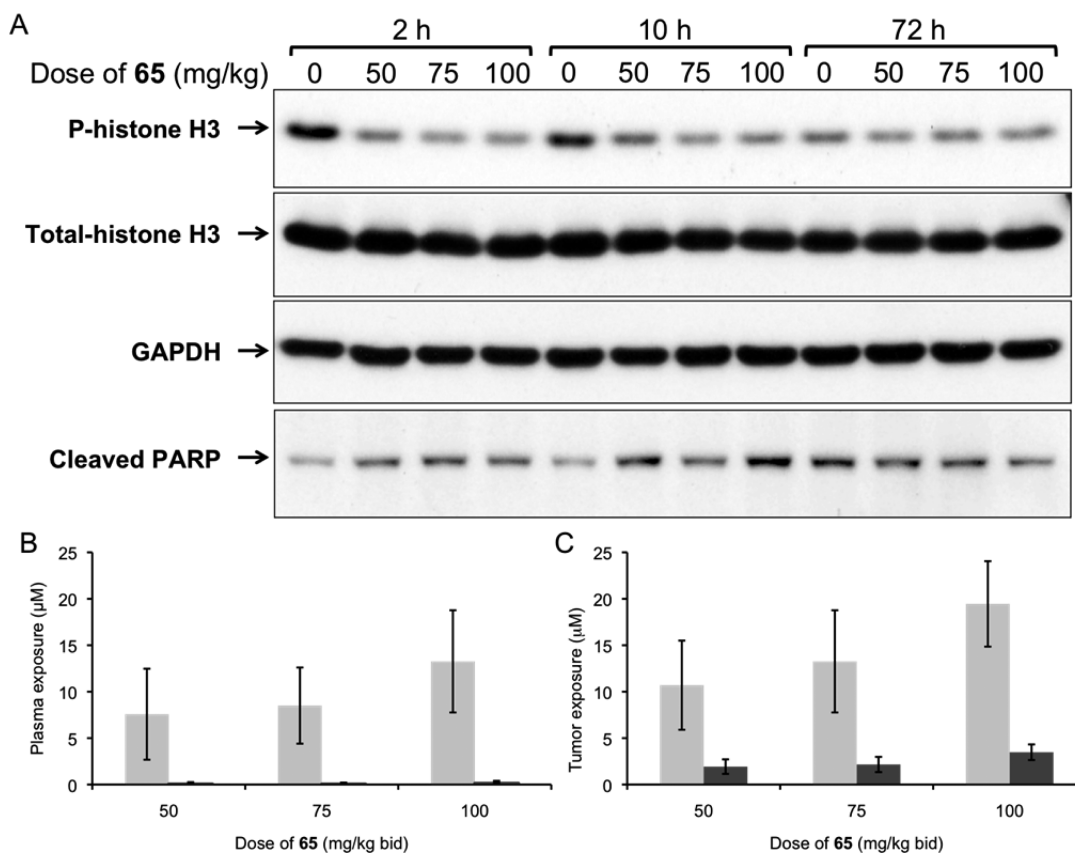


Figure 8. (A) Representative immunoblots of phospho-histone H3 showing dose-dependent PD modulation in HCT116 human tumor xenografts following two oral doses of **65** (50, 75, and 100 mg/kg) or vehicle. Total histone H3, cleaved poly ADP ribose polymerase (PARP, a measure of apoptosis), and glyceraldehyde 3-phosphate dehydrogenase (GAPDH, for protein loading) are also shown. (B, C) Plasma and tumor exposure levels of **65** from the same experiment measured 2 (light gray bars) or 10 h (dark gray bars) after the last dose.

The mobile phase was a mixture of MeOH (solvent A) and water (solvent B), both containing formic acid at 0.1%. Gradient elution was as follows: 1:9 (A/B) to 9:1 (A/B) over 2.5 min, 9:1 (A/B) for 1 min, and then reversion back to 1:9 (A/B) over 0.3 min, and finally 1:9 (A/B) for 0.2 min (default method, also referred to as ESI-HRMS method B). The following reference masses were used for HRMS analysis: caffeine $[M + H]^+$ 195.087652, hexakis(1*H*,1*H*,3*H*-tetrafluoropentoxy)phosphazene $[M + H]^+$ 922.009798, and hexakis(2,2-difluoroethoxy)phosphazene $[M + H]^+$ 622.02896 or reserpine $[M + H]^+$ 609.280657. All tested compounds gave >95% purity as determined by either method A or method B.

Preparation of Compounds in Table 1 (Exemplified by the Preparation of Compound 3). 2-Bromo-5-iodopyridin-4-amine (**15**). 4-Amino-2-bromopyridine **13** (22.8 g, 131.8 mmol) and sodium acetate (20.8 g, 254 mmol) were stirred in AcOH (82 mL), and a solution of iodine monochloride (1 M in AcOH, 134 mL, 134 mmol) was added. The mixture was stirred and heated at 75 °C for 3 h. Most of the AcOH was evaporated, and the residue was partitioned between water and EtOAc. The aqueous fraction was again extracted with EtOAc. The combined extracts were washed twice with 10% sodium carbonate solution, 10% sodium thiosulfate solution, water, and brine, dried, and evaporated. This gave 40.3 g of a crude product that was combined with the product from a reaction on 7.5 g of 4-amino-2-bromopyridine. Purification by chromatography on a silica column (9 cm internal diameter with 28 cm bed of silica) eluting with 5% EtOAc in CH₂Cl₂, then 10% EtOAc in CH₂Cl₂, and then 20% EtOAc in CH₂Cl₂ gave desired isomer **15** (20.2 g, 38%). ¹H NMR (500 MHz, CDCl₃): δ 4.74 (br s, 2H, NH₂), 6.80 (s, 1H), 8.34 (s, 1H). LC (method A)-MS (ESI, *m/z*) *t*_R 1.82 min, 299 [(*M* + *H*⁺), 100%] and subsequently with EtOAc/CH₂Cl₂ (1:1) to give undesired isomer 4-amino-2-bromo-3-iodopyridine **14** (19.3 g, 37%). LC (method A)-MS (ESI, *m/z*) *t*_R 1.62 min, 299 [(*M* + *H*⁺), 100%].

N-(2-Bromo-5-iodopyridin-4-yl)methanesulfonamide (**16**). 4-Amino-2-bromo-5-iodopyridine **15** (3.055 g, 10.2 mmol) was stirred in CH₂Cl₂ (34 mL), and Et₃N (6.9 mL, 49.1 mmol) was added. The mixture was cooled in ice. To the cold solution was added dropwise a solution of methanesulfonyl chloride (3.2 mL, 40.6 mmol) in CH₂Cl₂ (11.5 mL) over a period of 14 min. The cold bath was removed, and the reaction was stirred at rt for 1.5 h. The reaction was diluted with CH₂Cl₂ and washed twice with water. The solution was dried and evaporated. Trituration with ether gave a solid (5.01 g). The crude product was passed in 5% EtOAc in CH₂Cl₂ through a 2.5 cm pad of silica in a 10 cm diameter sinter to give *N*-(2-bromo-5-iodopyridin-4-yl)-*N*-(methylsulfonyl)methanesulfonamide (3.01 g, 64%). ¹H NMR (500 MHz, CDCl₃): δ 3.60 (s, 6H), 7.53 (s, 1H), 8.89 (s, 1H). LC (method A)-MS (ESI, *m/z*) *t*_R 1.91 min, 455 [(*M* + *H*⁺), 100%]. *N*-(2-Bromo-5-iodopyridin-4-yl)-*N*-(methylsulfonyl)methanesulfonamide (228 mg, 0.50 mmol) was stirred with THF (1.3 mL) and 10% sodium hydroxide in water (1.3 mL) at rt for 3 h. The THF was evaporated, and the aqueous phase was neutralized using a 10% citric acid solution. The deposited white solid was filtered off, washed with water, and dried in a vacuum desiccator over sodium hydroxide to give **16** (159 mg, 84%). ¹H NMR (500 MHz, DMSO-*d*₆): δ 3.29 (s, 3H), 7.54 (s, 1H), 8.64 (s, 1H). LC (method A)-MS (ESI, *m/z*) *t*_R 1.89 min, 377 [(*M* + *H*⁺), 100%].

tert-Butyl 4-((Trimethylsilyl)ethynyl)-1*H*-pyrazole-1-carboxylate (**19**). 4-Iodopyrazole **18** (7.85 g, 40.4 mmol) was dissolved in THF (120 mL), and Et₃N (8.5 mL, 60.5 mmol) and di-*tert*-butyl dicarbonate (9.7 g, 44.5 mmol) were added. The reaction was stirred at rt for 3 h. The THF was evaporated, and EtOAc was added. The solution was washed with water and brine, dried, and evaporated to leave an oil (14.2 g). The crude product was purified by chromatography on a pad of silica in a sinter (10 cm diameter, 6 cm thick) eluted with 10% EtOAc in cyclohexane and then 20%

EtOAc in cyclohexane to give *tert*-butyl 4-iodo-1*H*-pyrazole-1-carboxylate (11.66 g, 98%). ¹H NMR (500 MHz, CDCl₃): δ 1.68 (s, 9H), 7.73 (s, 1H), 8.17 (s, 1H). *tert*-Butyl 4-iodo-1*H*-pyrazole-1-carboxylate (4.67 g, 15.9 mmol) and trimethylsilylacetylene (2.18 g, 22.2 mmol) were dissolved in DMF (22 mL) and placed under argon. Diisopropylamine (2.9 mL, 20.7 mmol), copper(I) iodide (197 mg, 1.03 mmol), triphenylphosphine (832 mg, 3.18 mmol), and palladium acetate (239 mg, 1.06 mmol) were added, and the flask was flushed again with argon. The reaction was heated at 60 °C for 1.25 h. The reaction was cooled and added to water. The product was extracted with ether. The combined extracts were washed with water and brine, dried, and evaporated. The crude product was purified by flash chromatography (silica, eluting with 10% EtOAc in cyclohexane) to give **19** (3.88 g, 92%). ¹H NMR (500 MHz, CDCl₃): δ 0.25 (s, 6H), 1.67 (s, 9H), 7.77 (d, *J* = 0.6 Hz, 1H), 8.20 (d, *J* = 0.6 Hz, 1H).

tert-Butyl 4-Ethynyl-1*H*-pyrazole-1-carboxylate (**20**). *tert*-Butyl 4-((trimethylsilyl)ethynyl)-1*H*-pyrazole-1-carboxylate **19** (3.88 g, 14.69 mmol) was dissolved in THF (40 mL) and cooled to 0–5 °C. A 1 M solution of tetrabutylammonium fluoride in THF (16 mL, 16 mmol) was added, and the reaction was stirred for 20 min. The THF was evaporated, and the residue was taken up in EtOAc and washed with water and brine, dried, and evaporated. The residue was purified on a flash column (silica, eluting with 15% EtOAc in cyclohexane) to give **20** (1.765 g, 62%). ¹H NMR (500 MHz, CDCl₃): δ 1.68 (s, 9H), 3.11 (s, 1H), 7.79 (s, 1H), 8.24 (s, 1H). LC (method A)-MS (ESI, *m/z*) *t*_R 2.27 min, no ion recorded.

tert-Butyl 6-Bromo-2-(1-(*tert*-butoxycarbonyl)-1*H*-pyrazol-4-yl)-1*H*-pyrrolo[3,2-*c*]pyridine-1-carboxylate (**17**). To a mixture of *N*-(2-bromo-5-iodopyridin-4-yl)methanesulfonamide **16** (419 mg, 1.11 mmol) and *tert*-butyl-4-ethynyl-1*H*-pyrazole-1-carboxylate **20** (277 mg, 1.44 mmol) were added copper(I) iodide (7.4 mg, 0.039 mmol) and DMF (4 mL) followed by Et₃N (0.69 mL, 4.92 mmol). The reaction was flushed with nitrogen. Bis(triphenylphosphine)palladium dichloride (27 mg, 0.038 mmol) was added, the reaction flushed with nitrogen, and it was heated at 60 °C for 70 min. The reaction was added to water and extracted with EtOAc. The combined extracts were washed with water and brine, dried, and evaporated. The residue was purified on four 2 mm, 20 × 20 cm silica prep TLC plates and eluted with EtOAc/cyclohexane (3:1). The product band was recovered with acetone to give *tert*-butyl 4-(6-bromo-1-(methylsulfonyl)-1*H*-pyrrolo[3,2-*c*]pyridin-2-yl)-1*H*-pyrazole-1-carboxylate (251 mg, 51%). ¹H NMR (500 MHz, CDCl₃): δ 1.73 (s, 9H), 3.02 (s, 3H), 6.81 (s, 1H), 7.97 (s, 1H), 8.26 (s, 1H), 8.43 (s, 1H), 8.69 (s, 1H). LC (method A)-MS (ESI, *m/z*) *t*_R 2.55 min, 441 [(*M* + *H*⁺), 100%]. *tert*-Butyl-4-(6-bromo-1-(methylsulfonyl)-1*H*-pyrrolo[3,2-*c*]pyridin-2-yl)-1*H*-pyrazole-1-carboxylate (1.48 g, 3.35 mmol) was stirred in THF (20 mL), and DBU (0.51 mL, 3.4 mmol) was added. The reaction was warmed at 40 °C for 1 h. The reaction was cooled, and THF was evaporated. The residue was dissolved in EtOAc (50 mL), washed with water and brine, dried, and evaporated. ¹H NMR of the residue revealed incomplete conversion. The material was redissolved in THF (20 mL), and DBU (0.3 mL) was added. The reaction was heated at 40 °C for 1.5 h. MeOH (1 mL) was added, and heating was continued for 0.5 h. The solution was evaporated, and EtOAc was added. The solution was washed with water. The organic solution was washed again with water and brine, dried, and evaporated. ¹H NMR of the residue revealed both demethylated and completely deprotected products. To this material were added EtOAc and di-*tert*-butyl dicarbonate (1.11 g, 5.1 mmol) followed by Et₃N (0.72 mL, 5.1 mmol) and a crystal of DMAP. The reaction was stirred at rt for 1 h, more di-*tert*-butyl dicarbonate (414 mg, 1.9 mmol) was added, and stirring was continued for a further 2 h. The solution was evaporated, and the residue was kept at ambient temperature overnight. It was adsorbed from CH₂Cl₂ onto flash silica, packed onto a flash column made in 20% EtOAc in cyclohexane, and eluted with this solvent and then with 40% EtOAc in cyclohexane to give **17** (1.2 g, 77%). ¹H NMR (500 MHz, CDCl₃): δ 1.58 (s, 9H), 1.69 (s, 9H), 6.67 (d, *J* = 1.0 Hz, 1H), 7.84 (d, *J* = 1.0 Hz, 1H), 8.24 (t, *J* = 0.6 Hz, 1H), 8.27 (d, *J* = 0.6 Hz, 1H), 8.61 (d, *J* = 0.6 Hz, 1H). LC (method B)-MS (ESI, *m/z*) *t*_R 3.31 min, 407 [(*M* + *H*⁺-C₄H₈), 100%].

N-(3,4-Dimethoxyphenyl)-2-(1*H*-pyrazol-4-yl)-1*H*-pyrrolo[3,2-*c*]pyridin-6-amine (**8**). To *tert*-butyl 6-bromo-2-(1-(*tert*-butoxycarbonyl)-1*H*-pyrazol-4-yl)-1*H*-pyrrolo[3,2-*c*]pyridine-1-carboxylate **17** (101 mg, 0.218 mmol) was added 3,4-dimethoxyaniline (42 mg, 0.275 mmol) followed by cesium carbonate (140 mg, 0.432 mmol) and Xantphos (12.4 mg, 0.0216 mmol). Dioxane (2.4 mL) was added, and the flask flushed with nitrogen. Tris(dibenzylideneacetone)-dipalladium(0) (10 mg, 0.0108 mmol) was added, and the flask was flushed again with nitrogen and heated at 80 °C for 5.25 h. The reaction was cooled and diluted with EtOAc. The solution was washed with water and brine, dried, and evaporated. The residue was applied in chloroform to three 1 mm, 20 × 20 cm silica prep plates that were eluted with CH₂Cl₂/EtOAc (9:1). The product band was recovered with acetone to give *tert*-butyl-2-(1-(*tert*-butoxycarbonyl)-1*H*-pyrazol-4-yl)-6-(3,4-dimethoxyphenylamino)-1*H*-pyrrolo[3,2-*c*]pyridine-1-carboxylate (91 mg, 77%). ¹H NMR (500 MHz, CDCl₃): δ 1.46 (s, 9H), 1.68 (s, 9H), 3.90 (s, 3H), 3.91 (s, 3H), 6.45 (br s, 1H), 6.56 (d, *J* = 1.0 Hz, 1H), 6.89 (m, 2H), 6.96 (m, 1H), 7.45 (m, 1H), 7.81 (d, *J* = 0.6 Hz, 1H), 8.20 (d, *J* = 1.0 Hz, 1H), 8.42 (d, *J* = 1.0 Hz, 1H). ESI-HRMS calcd for C₂₈H₃₄N₅O₆ [*M* + *H*⁺], 536.2504; found, 536.2528. *tert*-Butyl-2-(1-(*tert*-butoxycarbonyl)-1*H*-pyrazol-4-yl)-6-(3,4-dimethoxyphenylamino)-1*H*-pyrrolo[3,2-*c*]pyridine-1-carboxylate (88 mg, 0.164 mmol) was dissolved in CH₂Cl₂ (0.8 mL), TFA (0.8 mL) was added to the solution, and the mixture was stirred at rt for 3.5 h. The solution was evaporated, and the residue dried in vacuum over NaOH for 1 h. The residue was dissolved in MeOH, the solution was evaporated, and the residue again was dried in a vacuum desiccator. The glassy material was taken up in MeOH, and 1 M sodium hydroxide solution (180 μL, 0.18 mmol) was added. The solution was applied to a 2 g SCX-2 column, and the column washed with more MeOH. The product was recovered using 2 M ammonia in MeOH to give a gum after evaporation (56 mg). This was triturated with ether to give **8** as a solid (49 mg, 89%). ¹H NMR (500 MHz, DMSO-*d*₆): δ 3.74 (s, 3H), 3.74 (s, 3H), 6.50 (s, 1H), 6.72 (s, 1H), 6.84 (d, *J* = 8.5 Hz, 1H), 7.06 (dd, *J* = 8.5, 2.2 Hz, 1H), 7.21 (d, *J* = 2.2 Hz, 1H), 8.01 (s, 1H), 8.25 (s, 1H), 8.33 (s, 1H), 11.11 (br s, 1H), 12.96 (br s, 1H). ESI-HRMS calcd for C₁₈H₁₈N₅O₂ [*M* + *H*⁺], 336.1455; found, 336.1468.

Preparation of Compounds in Tables 2 and 5 (Exemplified by the Preparation of Compounds 39, 40, and 48). 4-Ethynyl-1-methyl-1*H*-pyrazole (**45**). 4-Iodopyrazole **18** (5.0 g, 25.7 mmol) was dissolved in DMF (50 mL), and potassium carbonate (4.26 g, 30.9 mmol) was added and stirred (2 min) before iodomethane (1.76 mL, 28.3 mmol) was added. The reaction was stirred rapidly at rt for 17 h. It was filtered through a Celite pad, and the filtrate was evaporated to 10 mL using a rotary evaporator. Water was added to the residue, and the resultant mixture was extracted with EtOAc. The combined organics were washed with water and brine, dried, and evaporated to give 1-methyl-4-iodopyrazole as a solid (4.56 g, 85%). ¹H NMR (500 MHz, CDCl₃): δ 3.93 (s, 3H), 7.42 (s, 1H), 7.50 (s, 1H). LC (method A)-MS (ESI, *m/z*) *t*_R 1.74 min, 209 [(*M* + *H*⁺), 100%]. 1-Methyl-4-iodo-pyrazole (5.0 g, 24.04 mmol) was dissolved in DMF (32 mL), and trimethylsilylacetylene (4.76 mL, 33.7 mmol) was added followed by diisopropylamine (4.46 mL, 31.78 mmol), copper(I) iodide (304 mg, 1.59 mmol), and triphenylphosphine (1.26 g, 4.81 mmol). The reaction was flushed with argon. Palladium acetate (351 mg, 1.56 mmol) was added, and the reaction was again flushed with argon. It was heated at 60 °C for 1 h. The reaction was cooled, added to water, and extracted with ether. The organic solution was filtered from a brown solid, which was washed with a little more ether. The organic solution was washed with water and brine, dried, and evaporated. The crude product was chromatographed (silica gel) using EtOAc/cyclohexane (1:4) and then EtOAc/cyclohexane (1:3) to give 1-methyl-4-((trimethylsilyl)ethynyl)-1*H*-pyrazole as a solid (2.85 g, 67%). ¹H NMR (500 MHz, CDCl₃): δ 0.24 (s, 9H), 3.87 (s, 3H), 7.50 (s, 1H), 7.58 (s, 1H). LC (method A)-MS (ESI, *m/z*) *t*_R 2.44 min, 179 [(*M* + *H*⁺), 100%]. 1-Methyl-4-((trimethylsilyl)ethynyl)-1*H*-pyrazole (6.86 g, 38.5 mmol) was dissolved in MeOH (77 mL), and potassium carbonate (385 mg, 2.79 mmol) was added. The reaction was stirred at rt for 2 h. MeOH was evaporated to a small volume. EtOAc was added, and the solution washed with water and brine. Each aqueous phase was

backwashed with a single 40 mL portion of EtOAc. The EtOAc solution was dried and evaporated, and the residue was chromatographed (silica) and eluted with EtOAc/cyclohexane (1:3) and EtOAc/cyclohexane (1:1) to give **45** (3.18 g, 77%). ¹H NMR (500 MHz, CDCl₃): δ 3.00 (s, 1H), 3.88 (s, 3H), 7.52 (s, 1H), 7.59 (s, 1H). LC (method A)-MS (ESI, *m/z*) *t_R* 1.34 min, no ion recorded.

2-Bromo-5-((1-methyl-1H-pyrazol-4-yl)ethynyl)pyridin-4-amine (46). 4-Amino-2-bromo-5-iodopyridine **15** (2.58 g, 8.63 mmol), copper(I) iodide (164 mg, 0.86 mmol), and bis(triphenylphosphine)palladium dichloride (216 mg, 0.432 mmol) were weighed into a 100 mL flask, and DMF (25 mL) with Et₃N (22 mL) was added. The mixture was stirred at rt for 15 min under nitrogen. 4-Ethynyl-1-methyl-1H-pyrazole **45** (945 mg, 8.91 mmol) in DMF (10 mL) and Et₃N (5 mL) were added to the flask. The reaction was stirred at rt for 1.75 h. The reaction was diluted with EtOAc, and the solution was washed with water and brine, dried, and evaporated. The residue was purified by flash chromatography (silica/EtOAc) to give **46** (2.11 g, 88%). ¹H NMR (500 MHz, CDCl₃): δ 3.94 (s, 3H), 4.80 (br s, 2H), 6.79 (s, 1H), 7.59 (s, 1H), 7.66 (s, 1H), 8.15 (s, 1H). LC (method A)-MS (ESI, *m/z*) *t_R* 1.83 min, 277 [(M + H)⁺], 100%.

tert-Butyl-6-bromo-2-(1-methyl-1H-pyrazol-4-yl)-1H-pyrrolo[3,2-c]pyridine-1-carboxylate (47). Potassium *tert*-butoxide (315 mg, 2.81 mmol) was dissolved in NMP (3 mL), and 2-bromo-5-((1-methyl-1H-pyrazol-4-yl)ethynyl)pyridin-4-amine **46** (375 mg, 1.35 mmol) was added to the stirred solution. The reaction was placed under nitrogen and warmed at 50 °C for 3 h. The reaction was cooled, and 10% ammonium chloride (3 mL) added. Water (21 mL) was heated to about 60 °C, and the product solution in NMP/water was added to the water; a solid immediately crashes out. The suspension was allowed to cool to rt and filtered, and the solid was washed with water. Drying in a vacuum desiccator over KOH for 3 days gave product (347 mg) that was azeotroped with EtOH and toluene to give 6-bromo-2-(1-methyl-1H-pyrazol-4-yl)-1H-pyrrolo[3,2-c]pyridine (315 mg, 84%). ¹H NMR (500 MHz, DMSO-*d*₆): δ 3.90 (s, 3H), 6.69 (d, *J* = 1.0 Hz, 1H), 7.47 (t, *J* = 1.0 Hz, 1H), 7.94 (d, *J* = 0.6 Hz, 1H), 8.18 (s, 1H), 8.50 (d, *J* = 1.0 Hz, 1H), 11.92 (br s, 1H). LC (method A)-MS (ESI, *m/z*) *t_R* 1.67 min, 277 [(M + H)⁺], 100%. 6-Bromo-2-(1-methyl-1H-pyrazol-4-yl)-1H-pyrrolo[3,2-c]pyridine (7.22 g, 26.1 mmol) was stirred in EtOAc (93 mL) and Et₃N (5.3 mL, 37.8 mmol). To the suspension were added DMAP (622 mg, 5.1 mmol) and di-*tert*-butyl dicarbonate (8.30 g, 38.1 mmol). After 25 min, solid was deposited from solution, and the suspension was evaporated to dryness. The residue was chromatographed (silica, EtOAc/cyclohexane (1:1) then EtOAc/cyclohexane (3:1) then pure EtOAc) to give **47** (8.8 g, 89%). ¹H NMR (500 MHz, CDCl₃): δ 1.57 (s, 9H), 3.98 (s, 3H), 6.57 (d, *J* = 0.6 Hz, 1H), 7.59 (s, 1H), 7.63 (d, *J* = 0.6 Hz, 1H), 8.19 (t, *J* = 0.6 Hz), 8.58 (d, *J* = 0.6 Hz, 1H). LC (method A)-MS (ESI, *m/z*) *t_R* 2.75 min, 321 [(M + H)⁺-C₄H₉], 100%.

tert-Butyl-6-(2-chloro-4-(dimethylcarbamoyl)phenylamino)-2-(1-methyl-1H-pyrazol-4-yl)-1H-pyrrolo[3,2-c]pyridine-1-carboxylate (48). Tris(dibenzylideneacetone)dipalladium(0) (6.2 mg, 6.76 μmol) was added to a mixture of *tert*-butyl 6-bromo-2-(1-methyl-1H-pyrazol-4-yl)-1H-pyrrolo[3,2-c]pyridine-1-carboxylate **47** (51 mg, 0.135 mmol), cesium carbonate (88 mg, 0.270 mmol), 4-amino-3-chloro-*N,N*-dimethylbenzamide (32 mg, 0.162 mmol), and Xantphos (7.8 mg, 0.014 mmol) in dioxane (1.5 mL). The vial was flushed with dry argon, and the reaction mixture was heated at 80 °C for 3 h. Another 0.2 equiv of Pd and 0.4 equiv of ligand were added, and the reaction mixture was heated at 80 °C for 3 h. The reaction mixture was then filtered on SCX-2 column and concentrated under vacuum. The residue was purified via Biotage silica gel column chromatography, eluting with CH₂Cl₂/EtOH (99:1 to 90:10) to afford **48** as a white solid (19 mg, 28%). ¹H NMR (500 MHz, CDCl₃): δ 1.52 (s, 9H), 3.10 (s, 6H), 3.98 (s, 3H), 6.53 (s, 1H), 7.08 (s, 1H), 7.34 (dd, *J* = 8.5, 1.9 Hz, 1H), 7.55 (d, *J* = 1.9 Hz, 1H), 7.56 (s, 1H), 7.61 (s, 1H), 7.72 (s, 1H), 8.15 (d, *J* = 8.5 Hz, 1H), 8.53 (s, 1H). ESI-HRMS calcd for C₂₅H₂₈ClN₆O₃ [(M+H)⁺], 495.1906; found, 495.1900.

3-Chloro-*N,N*-dimethyl-4-(2-(1-methyl-1H-pyrazol-4-yl)-1H-pyrrolo[3,2-c]pyridin-6-ylamino)benzamide (39). *tert*-Butyl 6-(2-chloro-4-(dimethylcarbamoyl)phenylamino)-2-(1-methyl-1H-pyrazol-4-yl)-1H-pyrrolo[3,2-c]pyridine-1-carboxylate **48** (19 mg, 0.038 mmol) in

TFA (400 μL) was stirred for 30 min at rt. It was then concentrated and filtered on an Isolute Flash NH₂ column to afford **39** as a white solid (15 mg, 99%). ¹H NMR (500 MHz, CD₃OD): δ 3.08 (s, 6H), 3.95 (s, 3H), 6.62 (s, 1H), 7.10 (s, 1H), 7.27 (dd, *J* = 8.5, 2.0 Hz, 1H), 7.51 (d, *J* = 2.0 Hz, 1H), 7.61 (d, *J* = 8.5 Hz, 1H), 7.86 (s, 1H), 7.97 (s, 1H), 8.44 (s, 1H). ESI-HRMS calcd for C₂₀H₂₀ClN₆O [(M+H)⁺], 395.1382; found, 395.1370.

3-Methoxy-*N,N*-dimethyl-4-(2-(1-methyl-1H-pyrazol-4-yl)-1H-pyrrolo[3,2-c]pyridin-6-ylamino)benzamide (40). Tris(dibenzylideneacetone)dipalladium(0) (24.8 mg, 0.027 mmol) was added to a mixture of *tert*-butyl 6-bromo-2-(1-methyl-1H-pyrazol-4-yl)-1H-pyrrolo[3,2-c]pyridine-1-carboxylate **47** (51 mg, 0.135 mmol), cesium carbonate (88 mg, 0.270 mmol), 4-amino-3-methoxy-*N,N*-dimethylbenzamide (32 mg, 0.162 mmol), and Xantphos (31 mg, 0.054 mmol) in dioxane (1.5 mL). The vial was flushed with dry argon, and the reaction mixture was heated at 80 °C for 6 h. It was then filtered on a SCX-2 column and concentrated under vacuum. The residue was purified via Biotage silica gel column chromatography, eluting with CH₂Cl₂/EtOH (99:1 to 90:10) to afford *tert*-butyl-6-(4-(dimethylcarbamoyl)-2-methoxyphenylamino)-2-(1-methyl-1H-pyrazol-4-yl)-1H-pyrrolo[3,2-c]pyridine-1-carboxylate as a white solid (13 mg, 20%). ¹H NMR (500 MHz, CDCl₃): δ 1.52 (s, 9H), 3.11 (s, 6H), 3.95 (s, 3H), 3.97 (s, 3H), 6.50 (s, 1H), 7.05 (dd, *J* = 8.2, 1.7 Hz, 1H), 7.08 (d, *J* = 1.7 Hz, 1H), 7.22 (s, 1H), 7.54 (s, 1H), 7.60 (s, 1H), 7.69 (s, 1H), 8.10 (d, *J* = 8.2 Hz, 1H), 8.49 (s, 1H). LC (method B)-MS (ESI, *m/z*) *t_R* 2.40 min, 491 [(M + H)⁺], 100%. *tert*-Butyl-6-(4-(dimethylcarbamoyl)-2-methoxyphenylamino)-2-(1-methyl-1H-pyrazol-4-yl)-1H-pyrrolo[3,2-c]pyridine-1-carboxylate (13 mg, 0.027 mmol) in TFA (265 μL) was stirred for 30 min at rt. It was then concentrated and filtered on an Isolute Flash NH₂ column. The residue was purified via Biotage silica gel column chromatography, eluting with 10% MeOH/aq NH₃ (10:1) in CH₂Cl₂ to afford **40** as a white solid (7 mg, 68%). ¹H NMR (500 MHz, CD₃OD): δ 3.11 (s, 6H), 3.95 (s, 3H), 3.96 (s, 3H), 6.59 (d, *J* = 0.8 Hz, 1H), 7.01 (dd, *J* = 8.2, 1.8 Hz, 1H), 7.06–7.09 (m, 2H), 7.65 (d, *J* = 8.2 Hz, 1H), 7.85 (s, 1H), 7.95 (s, 1H), 8.40 (d, *J* = 0.8 Hz, 1H). ESI-HRMS calcd for C₂₁H₂₃N₆O₂ [(M+H)⁺], 391.1877; found, 391.1873.

4-Amino-3-methoxy-*N,N*-dimethylbenzamide. HATU (0.296 g, 0.778 mmol) was added to a solution of 4-amino-3-methoxybenzoic acid (0.1 g, 0.598 mmol), DIPEA (0.15 mL, 0.897 mmol), and dimethylamine (2 M in THF, 0.60 mL, 1.196 mmol) in THF (1.6 mL) under argon. The reaction mixture was stirred overnight. It was then partitioned between EtOAc and water. The separated organic phase was washed with water, dried over Na₂SO₄, and evaporated in vacuum. The crude was purified via Biotage silica gel column chromatography, eluting with CH₂Cl₂/EtOAc (60:40 to 40:60), and was then filtered on a SCX-2 column to afford the title compound as a colorless oil (69 mg, 59%). ¹H NMR (500 MHz, CDCl₃): δ 3.06 (s, 6H), 3.87 (s, 1H), 3.99 (br s, 2H), 6.65 (d, *J* = 7.9 Hz, 1H), 6.89 (dd, *J* = 7.9, 1.7 Hz, 1H), 6.96 (d, *J* = 1.7 Hz). LC (method B)-MS (ESI, *m/z*) *t_R* 1.23 min, 195 [(M + H)⁺], 100%.

Preparation of Compounds in Scheme 5 (Exemplified by Compounds 34 and 55). **6-Bromo-2-(diethoxymethyl)-1-(methylsulfonyl)-1H-pyrrolo[3,2-c]pyridine (57)**. To DMF (3.4 mL) containing Et₃N (0.64 mL, 4.5 mmol) were added propargylaldehyde diethyl acetal **56** (183 μL, 1.27 mmol) and *N*-(2-bromo-5-iodopyridin-4-yl)-methanesulfonamide **16** (400 mg, 1.06 mmol) followed by copper(I) iodide (7.1 mg, 0.037 mmol). The reaction was placed under nitrogen. Bis(triphenylphosphine)palladium dichloride (26.1 mg, 0.037 mmol) was added, and the reaction was flushed again with nitrogen and then heated at 60 °C for 2 h. The reaction was cooled and added to water containing a NaHCO₃ solution. The reaction was extracted with EtOAc. The combined organic layers were washed with water containing NaHCO₃ solution and brine, and concentrated in vacuo. The residue was purified using silica gel column chromatography, eluting with 100% CH₂Cl₂ to 5% EtOAc in CH₂Cl₂ to 10% EtOAc in CH₂Cl₂ to give **57** (207 mg, 51%). ¹H NMR (500 MHz, CDCl₃): δ 1.32 (t, *J* = 6.9 Hz, 6H), 3.38 (s, 3H), 3.75 (m, 2H), 3.84 (m, 2H), 5.86 (d, *J* = 1.0 Hz, 1H), 6.94 (t, *J* = 1.0 Hz, 1H), 8.14 (t, *J* = 1.0 Hz, 1H),

8.67 (d, $J = 1.0$ Hz, 1H). LC (method A)-MS (ESI, m/z) t_R 2.44 min, 377 [(M + H⁺), 100%].

6-Bromo-2-(diethoxymethyl)-1H-pyrrolo[3,2-c]pyridine (58). 6-Bromo-2-(diethoxymethyl)-1-(methylsulfonyl)-1H-pyrrolo[3,2-c]pyridine **57** (202 mg, 0.54 mmol) was stirred in MeOH (2.4 mL), and 1 M sodium hydroxide in water (0.62 mL, 0.62 mmol) was added. The reaction was stirred at 25 °C for 6 h. The MeOH was evaporated, and the residue taken up in EtOAc. The solution was washed with water and brine, and the organic layer was concentrated in vacuo to afford **58** (142 mg, 89%). ¹H NMR (500 MHz, CDCl₃): δ 1.27 (t, $J = 6.9$ Hz, 6H), 3.58–3.72 (m, 4H), 5.73 (m, 1H), 6.59 (m, 1H), 7.48 (m, 1H), 8.65 (s, 1H), 8.84 (br s, 1H). LC (method A)-MS (ESI, m/z) t_R 2.08 min, 253 [(M + H⁺-EtOH), 100%].

5-(6-Bromo-1H-pyrrolo[3,2-c]pyridin-2-yl)oxazole (59). To a solution of 6-bromo-2-(diethoxymethyl)-1H-pyrrolo[3,2-c]pyridine **58** (142 mg, 0.47 mmol) in THF (1.4 mL) and water (0.28 mL) was added tosic acid hydrate (134 mg, 0.705 mmol), and the reaction was stirred at 25 °C for 55 min. The reaction was partitioned between EtOAc and NaHCO₃. The layers were separated, and the aqueous layer again was extracted with EtOAc. The combined organic layers were washed with NaHCO₃ and brine and concentrated in vacuo to afford 6-bromo-1H-pyrrolo[3,2-c]pyridine-2-carbaldehyde (112 mg, over theory, residual solvent). ¹H NMR (500 MHz, CDCl₃): δ 7.37 (s, 1H), 7.62 (t, $J = 1.0$ Hz, 1H), 8.88 (d, $J = 1.0$ Hz, 1H), 9.32 (br s, 1H), 9.93 (s, 1H). LC (method A)-MS (ESI, m/z) t_R 1.59 min, 225 [(M + H⁺), 100%]. 6-Bromo-1H-pyrrolo[3,2-c]pyridine-2-carbaldehyde (604 mg, 2.68 mmol), TOSMIC (1.05 g, 5.37 mmol), and potassium carbonate (759 mg, 5.5 mmol) in MeOH (30 mL) was stirred and heated at 65 °C for 110 min. The MeOH was evaporated, and the residue was partitioned between EtOAc and water. The layers were separated, and the organic solution was washed with water and brine and concentrated in vacuo. The residue was purified using silica gel column chromatography, eluting with EtOAc to afford **59** (561 mg, 79%). ¹H NMR (500 MHz, acetone-*d*₆): δ 7.02 (d, $J = 1.0$ Hz, 1H), 7.60 (t, $J = 1.0$ Hz, 1H), 7.62 (s, 1H), 8.30 (s, 1H), 8.67 (d, $J = 1.0$ Hz, 1H). LC (method A)-MS (ESI, m/z) t_R 1.83 min, 264 [(M + H⁺), 100%].

tert-Butyl 6-Bromo-2-(oxazol-5-yl)-1H-pyrrolo[3,2-c]pyridine-1-carboxylate (60). 5-(6-Bromo-1H-pyrrolo[3,2-c]pyridin-2-yl)oxazole **59** (152 mg, 0.58 mmol) was stirred in EtOAc (2 mL). Et₃N (140 μ L, 1.0 mmol) was added followed by a crystal of DMAP and di-*tert*-butyl dicarbonate (190 mg, 0.87 mmol). The reaction was stirred at 25 °C for 60 min. Further di-*tert*-butyl dicarbonate (54 mg, 0.25 mmol) was added, and the reaction allowed to stir at rt overnight. The reaction was concentrated in vacuo, and the residue applied in chloroform to a preparative TLC plate. The product was eluted with EtOAc/cyclohexane (1:1, three times) to afford **60** (150 mg, 71%). ¹H NMR (500 MHz, CDCl₃): δ 1.54 (s, 9H), 6.90 (d, $J = 1.0$ Hz, 1H), 7.40 (s, 1H), 8.02 (s, 1H), 8.31 (s, 1H), 8.68 (s, 1H); LC (method A)-MS (ESI, m/z) t_R 2.58 min, 308 [(M + H⁺-C₄H₈), 100%].

N-(2-Methoxyphenyl)-2-(oxazol-5-yl)-1H-pyrrolo[3,2-c]pyridin-6-amine (34). To *tert*-butyl 6-bromo-2-(oxazol-5-yl)-1H-pyrrolo[3,2-c]pyridine-1-carboxylate **60** (49 mg, 0.135 mmol) were added cesium carbonate (88 mg, 0.27 mmol) and Xantphos (7.8 mg, 0.0135 mmol) and then 2-methoxyaniline (20 mg, 0.163 mmol) in dioxane (1.5 mL). The flask was flushed with nitrogen. Tris(dibenzylideneacetone)-dipalladium(0) (6.3 mg, 0.0068 mmol) was added, and the flask was flushed again with nitrogen and heated at 80 °C for 3 h. The reaction was cooled and diluted with EtOAc. The organic solution was washed with water and brine, dried, and evaporated. The residue was applied to two 1 mm, 20 × 20 cm silica prep TLC plates, which were eluted with EtOAc. The product band was recovered with acetone to afford *tert*-butyl-6-(2-methoxyphenylamino)-2-(oxazol-5-yl)-1H-pyrrolo[3,2-c]pyridine-1-carboxylate (44 mg, 80%). ¹H NMR (500 MHz, CDCl₃): δ 1.50 (s, 9H), 3.92 (s, 3H), 6.80 (d, $J = 0.6$ Hz, 1H), 6.92–7.02 (m, 3H), 7.14 (br s, 1H), 7.30 (s, 1H), 7.70 (t, $J = 1.0$ Hz, 1H), 7.99 (m, 2H), 8.55 (d, $J = 1.0$ Hz, 1H). ESI-HRMS calcd for C₂₂H₂₃N₄O₄ [M+H]⁺, 407.1714; found, 407.1707. *tert*-Butyl-6-(2-methoxyphenylamino)-2-(oxazol-5-yl)-1H-pyrrolo[3,2-c]pyridine-1-carboxylate (44 mg) was dissolved in CH₂Cl₂ (1 mL) and TFA (1 mL) and stirred at rt for 3.25 h. The solvents were evaporated, and the residue was kept for

1.5 h in a vacuum desiccator over NaOH. The residue was partitioned between EtOAc and a saturated NaHCO₃ solution. The layers were shaken and separated, and the aqueous layer was washed with more EtOAc. The combined organics were dried and evaporated, leaving a solid residue (33 mg). This was triturated with ether to give, after removal of the mother liquors and drying, compound **34** (27 mg, 81%). ¹H NMR (500 MHz, DMSO-*d*₆): δ 3.86 (s, 3H), 6.78 (d, $J = 1.0$ Hz, 1H), 6.84–6.91 (m, 2H), 6.96 (t, $J = 1.0$ Hz, 1H), 6.98–7.01 (m, 1H), 7.53 (s, 1H), 7.70 (br s, 1H), 8.04–8.07 (m, 1H), 8.47 (s, 1H), 8.49 (s, 1H), 11.65 (br s, 1H). ESI-HRMS calcd for C₁₇H₁₅N₄O₂ [M+H]⁺, 307.1190; found, 307.1186.

tert-Butyl-6-(2-chloro-4-(dimethylcarbamoyl)phenylamino)-2-(oxazol-5-yl)-1H-pyrrolo[3,2-c]pyridine-1-carboxylate (55). To *tert*-butyl 6-bromo-2-(oxazol-5-yl)-1H-pyrrolo[3,2-c]pyridine-1-carboxylate **60** (49 mg, 0.135 mmol) were added cesium carbonate (88 mg, 0.27 mmol), Xantphos (7.8 mg, 0.0135 mmol), and 4-amino-3-methoxy-*N,N*-dimethylbenzamide (32.1 mg solids, 0.162 mmol) in DMA (1.5 mL). The flask was flushed with argon. Tris(dibenzylideneacetone)dipalladium(0) (6.3 mg, 0.0068 mmol) was added, and the flask was flushed again with argon and heated at 80 °C for 3 h. The reaction was cooled and added to water. The product was extracted with EtOAc. The combined organics were washed with water and with brine, dried, and evaporated. The residue was applied to two 1 mm, 20 × 20 cm silica prep TLC plates, which were eluted twice with EtOAc. The product band was recovered with acetone to give impure product (45 mg). This still contains some of the aniline. This material was applied to one 1 mm, 20 × 20 cm silica prep TLC plate, which was eluted twice with EtOAc/CH₂Cl₂ (1:1). The product was recovered with acetone, giving **55** (39 mg, 60%). ¹H NMR (500 MHz, CDCl₃): δ 1.50 (s, 9H), 3.10 (s, 6H), 6.84 (d, $J = 0.6$ Hz, 1H), 7.17 (br s, 1H), 7.37 (dd, $J = 8.5, 1.9$ Hz, 1H), 7.56 (d, $J = 1.9$ Hz, 1H), 7.77 (s, 1H), 8.01 (s, 1H), 8.21 (d, $J = 8.5$ Hz, 1H), 8.61 (d, $J = 1.0$ Hz, 1H). ESI-HRMS calcd for C₂₄H₂₅ClN₅O₄ [M+H]⁺, 482.1590; found, 482.1586.

Preparation of Compound 65. *tert*-Butyl 6-(2-chloro-4-(1-methyl-1H-imidazol-5-yl) phenylamino)-2-(1-methyl-1H-pyrazol-4-yl)-1H-pyrrolo[3,2-c]pyridine-1-carboxylate (**65**). Tris(dibenzylideneacetone)-dipalladium(0) (6.1 mg, 6.63 μ mol) was added to a mixture of *tert*-butyl 6-bromo-2-(1-methyl-1H-pyrazol-4-yl)-1H-pyrrolo[3,2-c]pyridine-1-carboxylate **47** (50 mg, 0.133 mmol), cesium carbonate (86 mg, 0.265 mmol), 2-chloro-4-(1-methyl-1H-imidazol-5-yl)aniline (33 mg, 0.159 mmol), and Xantphos (7.7 mg, 0.013 mmol) in DMA (1.4 mL). The vial was flushed with dry argon, and the reaction mixture was heated at 80 °C for 3 h. It was then filtered on a SCX-2 column and concentrated under vacuum. The residue was purified via Biotage silica gel column chromatography, eluting with CH₂Cl₂/EtOH (99:1 to 95:5) to afford **65** as a white solid (40 mg, 60%). ¹H NMR (500 MHz, CDCl₃): δ 1.52 (s, 9H), 3.69 (s, 3H), 3.98 (s, 3H), 6.53 (d, $J = 0.9$ Hz, 1H), 7.04 (s, 1H), 7.09 (br s, 1H), 7.27 (dd, $J = 8.5, 2.0$ Hz, 1H), 7.45 (d, $J = 2.0$ Hz, 1H), 7.53 (br s, 1H), 7.56 (s, 1H), 7.61 (s, 1H), 7.72 (t, $J = 0.9$ Hz, 1H), 8.18 (d, $J = 8.5$ Hz, 1H), 8.52 (d, $J = 0.9$ Hz, 1H). ESI-HRMS calcd for C₂₆H₂₇ClN₇O₂ [M+H]⁺, 504.1909; found, 504.1885.

2-Chloro-4-(1-methyl-1H-imidazol-5-yl)aniline. Tetrakis(triphenylphosphine)palladium (0.046 g, 0.039 mmol) was added to a solution of 2-chloro-4-(4,4,5,5-tetramethyl-1,3,2-dioxaborolan-2-yl)-aniline (0.1 g, 0.394 mmol), 5-iodo-1-methyl-1H-imidazole (0.123 g, 0.592 mmol), and sodium carbonate (0.125 g, 1.183 mmol) in DME/H₂O (3:1, 2.0 mL). The vial was flushed with dry argon, and the reaction mixture was heated at 135 °C for 1 h under microwave irradiation. It was then diluted with EtOAc and quenched with water. The layers were separated, and the aqueous layer was extracted with EtOAc. The combined organic layers were dried (Na₂SO₄), filtered, and concentrated under reduced pressure. The crude mixture was purified via Biotage silica gel column chromatography, eluting with CH₂Cl₂/EtOH (99:1 to 95:5) to afford the title product as a white solid (50 mg, 61%). ¹H NMR (500 MHz, CDCl₃): δ 3.62 (s, 3H), 4.23 (br s, 2H), 6.81 (d, $J = 8.3$ Hz, 1H), 7.01 (d, $J = 1.2$ Hz, 1H), 7.08 (dd, $J = 8.2, 2.0$ Hz, 1H), 7.27 (d, $J = 2.0$ Hz, 1H), 7.47 (s, 1H). LC (method B)-MS (ESI, m/z) t_R 0.93 min, 208 [(M + H⁺), 100%].

Protein Production for Full-Length MPS1. The coding sequence for full-length human MPS1 was amplified by PCR using a plasmid containing MPS1 as a template (kindly provided by the laboratory of Prof. Dr. Eric Nigg, University of Basel, Basel, Switzerland). The PCR product was inserted into a modified version of pFastBac1 that encodes an N-terminal 6× His-tag followed by a GST-tag and then an HRV 3C protease site. Recombinant baculovirus was generated according to Bac-to-Bac protocols (Invitrogen, Paisley, UK). For protein production, Sf9 insect cells were grown in sf-900 II media to a cell density of around 2×10^6 cells per milliliter and infected with 30–100 μL of virus per 10^7 cells. Infected cell cultures were harvested 3 days postinfection. Cell pellets were resuspended in 3 volumes of lysis buffer (50 mM HEPES, pH 7.4, 100 mM NaCl, 1 mM MgCl_2 , and 10% (v/v) glycerol) containing 1× complete EDTA-free protease inhibitors, 20 mM β -glycerophosphate, 10 mM NaF, 2 mM Na_3VO_4 , and 25 U/mL benzamide nuclease, and the resuspended cells were lysed by sonication. Following centrifugation, the supernatant was purified over 10 mL of Talon resin using a batch/gravity protocol, eluting with 5 column volumes (CV) of 50 mM HEPES, pH 7.0, 300 mM NaCl, 250 mM imidazole, 10% (v/v) glycerol, and 1× complete EDTA-free protease inhibitors. The Talon eluate was subsequently purified over a 5 mL GSTrap FF column equilibrated in GSH buffer A (10 mM HEPES, pH 7.0, 150 mM NaCl, 1 mM DTT, 0.1 mM EDTA, and 0.0001% Tween 20) and eluted with 4 CV of GSH Buffer B (GSH buffer A + 10 mM glutathione). N-terminal His and GST tags were removed by overnight incubation at 4 °C with HRV 3C protease. Cleaved protein was concentrated to 0.5 mL and applied to a Superdex 200 HR 10/30 column in series with a 5 mL GSTrap FF column that was equilibrated with 10 mM HEPES, pH 7.0, 150 mM NaCl, 1 mM DTT, 0.1 mM EDTA, and 0.0001% Tween 20. Selected fractions were pooled, concentrated to 1 to 2 mg/mL, and frozen.

MPS1 Kinase Assay. The enzyme reaction (10 μL total volume) was carried out in black 384-well low-volume plates containing full-length MPS1 (LifeTechnologies or in-house, in a range from 3 to 12.5 nM to obtain 10% total conversion during the assay), fluorescently-labeled peptide [H236, sequence: SFAM-DHTGFLTEYVATR-CONH₂, Pepceuticals Ltd., Enderby, UK] (5 μM), ATP (10 μM), either 1% (v/v) DMSO or the test compound (in the range from 0.25 nM to 100 μM in 1% (v/v) DMSO), and assay buffer (50 mM HEPES, pH 7.0, 0.02% (w/v) NaN_3 , 0.01% (w/v) BSA, 0.1 mM orthovanadate, 10 μM MgCl_2 , 1 μM DTT, and Roche protease inhibitor). The reaction was carried out for either 60 or 90 min at room temperature and stopped by the addition of buffer (10 μL) containing 20 mM EDTA and 0.05% (v/v) Brij-35, in 0.1 M HEPES-buffered saline (Free acid, Sigma, UK). The plate was read on a Caliper EZ reader II (PerkinElmer Life Sciences, Waltham, MA, USA). The reader provides a Software package ('Reviewer') that converts the peak heights into percent conversion by measuring both the product and substrate peaks, and it also allows selection of control wells that represent 0 and 100% inhibition, respectively. The percent inhibition of the compounds was calculated relative to the mean values of selected control wells. IC_{50} values were determined by testing the compounds at a range of concentrations from 0.25 nM to 100 μM . The percent inhibition at each concentration was then fitted to a four-parameter logistic fit using the Studies package (Dotmatics, Bishops Stortford, UK): $y = (a + ((b - a)/(1 + ((c/x^d)))))$, where a = asym min, b = asym max, c = IC_{50} , and d = Hill coefficient.

Aurora A and Aurora B Kinase Assays. The enzyme reactions (10 μL total volume) were carried out in black 384-well low-volume plates containing full-length AurB/INCENP complex (1 nM, Carna Biosciences, Japan) or N-terminal HIS-tagged AurA (5 nM, in-house), fluorescently-labeled peptide [FL-Peptide 21, PerkinElmer, sequence: SFAM-LRRASLG-CONH₂] (1.5 μM), ATP (15 or 20 μM), either 1% (v/v) DMSO or the test compound (in the range from 0.25 nM to 100 μM in 1% (v/v) DMSO), and assay buffer (50 mM Tris, pH 7.4, 200 mM NaCl, 5 mM MgCl_2 , 2 mM DTT, and 0.1% (v/v) Tween 20). The reaction was carried out for 60 min at room temperature and stopped by the addition of buffer (10 μL) containing 20 mM EDTA and 0.05% (v/v) Brij-35 in 0.1 M HEPES-buffered saline (Free acid, Sigma, UK). The plate was read on a Caliper EZ reader II (PerkinElmer).

The reader provides a Software package ('Reviewer') that converts the peak heights into percent conversion by measuring both the product and substrate peaks. The percentage inhibition was calculated relative to blank wells (containing no enzyme and 1% (v/v) DMSO). IC_{50} values were determined by testing the compounds at a range of concentrations from 0.25 nM to 100 μM . The percent inhibition at each concentration was then fitted to a four-parameter logistic fit using the Studies package (Dotmatics, Bishops Stortford, UK): $y = (a + ((b - a)/(1 + ((c/x^d)))))$, where a = asym min, b = asym max, c = IC_{50} , and d = Hill coefficient.

CDK2 Kinase Assay. The enzyme reaction (10 μL total volume) was carried out in black 384-well low-volume plates containing full-length CDK2/CyclinA complex (2 nM, LifeTechnologies), fluorescently-labeled peptide [FL-Peptide18, PerkinElmer, sequence: SFAM-QSPKKG-CONH₂] (1.5 μM), ATP (25 μM), either 1% (v/v) DMSO or the test compound (in the range from 0.25 nM to 100 μM in 1% (v/v) DMSO), and assay buffer (50 mM HEPES, pH 7.0, 0.02% (w/v) NaN_3 , 0.01% (w/v) BSA, 0.1 mM orthovanadate, 10 μM MgCl_2 , and 1 μM DTT). The reaction was carried out for 60 min at room temperature and stopped by the addition of buffer (10 μL) containing 20 mM EDTA and 0.05% (v/v) Brij-35 in 0.1 M HEPES-buffered saline (Free acid, Sigma, UK). The plate was read on a Caliper EZ reader II (PerkinElmer). The reader provides a Software package ('Reviewer') that converts the peak heights into percent conversion by measuring both the product and substrate peaks. The percentage inhibition was calculated relative to blank wells (containing no enzyme and 1% (v/v) DMSO). IC_{50} values were determined by testing the compounds at a range of concentrations from 0.25 nM to 100 μM . The percent inhibition at each concentration was then fitted to a four-parameter logistic fit using the Studies package (Dotmatics, Bishops Stortford, UK): $y = (a + ((b - a)/(1 + ((c/x^d)))))$, where a = asym min, b = asym max, c = IC_{50} , and d = Hill coefficient.

GSK3 β Kinase Assay. All GSK3 β percentage inhibitions at 1 μM were performed in duplicates by Invitrogen in a Z'LYTE activity assay using their SelectScreen biochemical kinase profiling service.

Cell Viability Assay. Cell proliferation assays were carried out by colorimetric 3-(4,5-dimethylthiazol-2-yl)-2,5-diphenyltetrazolium bromide (MTT) assay (Sigma). Briefly, cells were plated in 96-well plates at 1500 cells per well in 100 μL of culture medium in triplicate. On the next day, 2-fold dilutions of the compounds to be tested were made in culture medium so that when diluted 5× the final concentration in the wells ranged from 0 to 20 μM . Twenty-five microliters of compounds dilutions in the medium was added to 100 μL of cells and incubated at 37 °C and 5% CO_2 for 3 more days (72 h). Cells were then incubated with 40 μL of 5 mg/mL solution of MTT reagent at 37 °C for 3 h. Media was carefully removed, and crystals were dissolved in 100 μL of DMSO. The absorbance was measured at 570 nm with the Wallac VICTOR2 1420 multilabel counter (PerkinElmer), and analysis was performed to calculate the GI_{50} using GraphPad PRISM.

MSD Assay for MPS1 Autophosphorylation. Cellular IC_{50} values of MPS1 autophosphorylation inhibition were measured by an in-house electrochemiluminescence (Meso Scale Discovery, MSD) assay that measured phosphorylation of ectopic MPS1 at the Thr33 and Ser37 sites.^{36,37} On day 1, 3×10^4 HCT116 cells per well in a 96-well plate were reverse-transfected with 100 ng of wild-type Myc-MPS1 using Lipofectamine LTX (Invitrogen). On the next day, cells were treated with 50 ng/mL of nocodazole. On the following day, cells were treated with 2-fold dilutions of test compounds ranging from 0 to 10 μM for 2 h in the presence of 10 μM MG132. After treatment, cells were washed with PBS and lysed with 60 μL per well of complete lysis buffer (50 mM NaCl, 20 mM Tris, pH 7.5, 1 mM EDTA, 1 mM EGTA, 1% (v/v) Triton X100, 10 mM NaF, protease inhibitor tablet, and phosphatase inhibitor cocktails) on ice for 30 min with shaking. Cell lysates were mixed thoroughly by pipetting up and down, and 25 μL of lysate was loaded onto MSD plates that were pre-coated with total MPS1 antibody (mouse monoclonal, Invitrogen, cat. no. 35-9100) and blocked with 3% (w/v) BSA. After a 1 h incubation at room temperature on a shaker, plates were washed three times with MSD wash buffer, and 25 μL of pThr33/pSer37 antibody (Invitrogen, cat. no. 44-1325G) diluted in 1% (w/v) BSA was added followed by incubation for a further 1 h at room temperature. Plates

were washed again three times with MSD wash buffer and incubated with 25 μL of anti-rabbit sulfo-TAG antibody (Meso Scale Discovery, cat. no. R32AB) diluted in 1% (w/v) BSA for 1 h. After the final incubation, plates were washed three times with MSD wash buffer and read in the presence of 1 \times MSD read buffer. IC₅₀ values were determined using GraphPad PRISM.

Solubility Assays. Aqueous, fed-state-simulated intestinal fluid (FeSSIF) and fasted-state-simulated intestinal fluid (FaSSIF) solubilities were determined at Pharmorphix.

Crystal Structure Determination of MPS1 with Ligands. The kinase domain (residues 519–808) of MPS1 was produced in *E. coli* and purified as described previously.³⁸ Purified MPS1 was crystallized in the apo form at 18 °C using the sitting-drop vapor-diffusion method. The crystallization drops were composed of 2 μL of protein (8.9 mg/mL) and 2 μL of reservoir solution placed over 200 μL of reservoir solution of 30–45% (v/v) aqueous PEG300 in 48-well plates. Apo crystals typically grew in 72 h. For compounds **8**, **34**, **39**, **48**, and **55**, apo-protein crystals were soaked for 24 h at 18 °C in 4 μL drops composed of 1–10 mM compound in 35% (v/v) PEG300, 0.1 M HEPES, pH 7.5, and 5% (v/v) DMSO. Soaked protein crystals were briefly transferred to cryoprotectant solution containing 40% (v/v) PEG300, 0.1 M HEPES, pH 7.5, and 20% (w/v) ethylene glycol prior to cryocooling in liquid nitrogen.

MPS1 was cocrystallized with compound **65** by mixing 2 μL of protein solution, premixed with 1 mM **65** for 30 min on ice, with 2 μL of reservoir solution placed over 200 μL of reservoir solution consisting of 14% (w/v) PEG8000, 0.05 M magnesium acetate, and 0.1 M sodium acetate. Cocrystals of MPS1 with **65** formed within 72 h at 18 °C and were briefly transferred to a cryoprotectant solution containing 10% (w/v) PEG8000, 0.05 M magnesium acetate, 0.1 M sodium acetate, and 25% (v/v) glycerol prior to cryocooling in liquid nitrogen.

X-ray data were collected at Diamond Light Source, Oxfordshire, UK, at beamlines I04 and I04-1. Crystals belonged to the space group *I*222 and diffracted to a resolution between 2.36 and 2.80 Å. Data were integrated with MOSFLM^{39,40} or XDS⁴¹ and scaled and merged with AIMLESS.⁴² The structures were solved by molecular replacement using PHASER,^{40,43} and a publicly available MPS1 structure (PDB code 4B11)³⁸ with ligand and water molecules removed was used as the molecular replacement model. The protein–ligand structures were manually rebuilt in COOT⁴⁴ and refined with BUSTER⁴⁵ in iterative cycles. Ligand restraints were generated with grade⁴⁶ and Mogul.⁴⁷ The quality of the structures was assessed with MOLPROBITY.⁴⁸ The data collection and refinement statistics are presented in Supporting Information Table S2.

Mouse Liver Microsomal Stability. Compounds (10 μM) were incubated with male CD1 mouse liver microsomes (1 mg/mL) protein in the presence of 1 mM NADPH, 2.5 mM UDP-glucuronic acid (UDPGA), and 3 mM MgCl₂ in 10 mM PBS at 37 °C. Incubations were conducted for 0 and 30 min. Control incubations were generated by the omission of NADPH and UDPGA from the incubation reaction. The percentage of compound remaining was determined after analysis by LC/MS.

Human Liver Microsomal Stability. Compounds (10 μM) were incubated with mixed-gender pooled human liver microsomes (1 mg/mL) protein in the presence of 1 mM NADPH, 2.5 mM UDPGA, and 3 mM MgCl₂ in 10 mM PBS at 37 °C. Incubations were conducted for 0 and 30 min. Control incubations were generated by the omission of NADPH and UDPGA from the incubation reaction. The percentage of compound remaining was determined after analysis by LC/MS.

In Vivo Mouse PK. All procedures involving animals were carried out within The ICR's Animal Ethics Committee and national guidelines.⁴⁹ Mice (female Balb/C) were dosed po or iv (5 or 10 mg/kg) in 10% (v/v) DMSO and 5% (v/v) Tween 20 in saline. After administration, mice were culled at 5, 15, and 30 min and 1, 2, 4, 6, and 24 h. Blood was removed by cardiac puncture and centrifuged to obtain plasma samples. Plasma samples (100 μL) were added to the analytical internal standard (olomoucine; IS) followed by protein precipitation with 300 μL of methanol. Following centrifugation (1200g, 30 min, 4 °C), the resulting supernatants were analyzed for

compound levels by LC/MS. For blood pharmacokinetics, 20 μL was spotted on a Whatman B card and allowed to dry for at least 12 h at room temperature and 6 mm diameter disks were punched and extracted with 200 μL of methanol containing 500 nM olomoucine used as internal standard. Sample extracts were analyzed by LC/MSMS against calibration curves (six levels) and six quality controls (three levels in duplicate). Separation was carried out by an Acquity UPLC binary system (Waters) on a reverse-phase Kinetex C18 (Phenomenex 50 \times 2.1 mm, 1.7 μm particles) analytical column. Elution was achieved with a 4.5 min gradient of 0.1% formic acid/methanol (95% formic acid to 0%) following a 0.5 min isocratic period. Detection was performed in positive ion mode ESI multiple-reaction monitoring (MRM) on a QTRAP 4000 (AB-SCIEX).

In Vivo Mouse PK/PD Study. Human HCT116 colon carcinoma cells (3×10^6) were sc injected bilaterally in the flanks of female CrTac:NCr-Fox1(*nu*) athymic mice. Once tumors reached a mean diameter of \sim 8 mm (day 15), mice were dosed twice at a 12 h intervals with 50, 75, or 100 mg/kg of compound **65** in 10% (v/v) DMSO and 5% (v/v) Tween 20 in saline. Mice were culled ($n = 3$ per group) at 2, 10, and 72 h after the second dose. Tumors were snap-frozen and stored at -80 °C until analysis. Tumor samples were homogenized in PBS (3 vol/tumor weight).

■ ASSOCIATED CONTENT

📄 Supporting Information

Experimental procedures for compounds **4–6**, **21–33**, **35–38**, **41–44**, **49–54**, **61–64**, and **66–68**. Scheme depicting slow air oxidation of compound **8**. Summary of kinase selectivity profiling of compound **65**. Crystallographic analysis of compounds **8**, **34**, **39**, **48**, **55**, and **65**. This material is available free of charge via the Internet at <http://pubs.acs.org>.

Accession Codes

Atomic coordinates and structure factors for the crystal structures of MPS1 with compounds **8**, **34**, **39**, **48**, **55**, and **65** can be accessed using PDB codes 4c4e, 4c4f, 4c4g, 4c4h, 4c4i, and 4c4j, respectively. In the deposited structure of MPS1 soaked with compound **39** (4c4g), the pyrrolo N-1-Boc substituted analogue **48** has been modeled.

■ AUTHOR INFORMATION

Corresponding Authors

*Telephone: +44(0)2087224364; E-mail: rob.vanmontfort@icr.ac.uk (R.L.M.v.M.).

*Telephone: +44(0)2087224051; E-mail: julian.blagg@icr.ac.uk (J.B.).

Notes

The authors declare the following competing financial interest(s): The authors are current or former employees of The Institute of Cancer Research, which has a commercial interest in the development of kinase inhibitors.

■ ACKNOWLEDGMENTS

This work was supported by Cancer Research UK grant numbers C309/A8274 and C309/A11566. S.L. is also supported by Breakthrough Breast Cancer. We acknowledge NHS funding to the NIHR Biomedical Research Centre at The Institute of Cancer Research and the Royal Marsden Hospital. We are grateful to Stefan Knapp, Structural Genomics Consortium, Oxford, UK, for the generous gift of expression plasmids for the kinase domain of MPS1 and Eric Nigg, University of Basel, Basel, Switzerland, for the construct of full-length MPS1. We thank Krishna Bulusu for his help with the “spine analysis” probing of the MPS1 conformation in our crystal structures. We thank Dr. Nora Cronin and the staff of

DIAMOND Light Source for their support during data collection. We also thank Dr. Amin Mirza, Mr Meirion Richards, and Dr. Manjuan Liu for their assistance with NMR, mass spectrometry, and HPLC.

■ ABBREVIATIONS USED

Cl, clearance; Cl_u, unbound clearance; DIPEA, *N,N*-diisopropylethylamine; GSK3 β , glycogen synthase kinase 3 β ; GAPDH, glyceraldehyde 3-phosphate dehydrogenase; HEPES, 4-(2-hydroxyethyl)piperazine-1-ethanesulfonic acid; HLM, human liver microsomes; JNK, c-Jun amino terminal kinase; LRRK2, leucine rich repeat kinase 2; MLM, mouse liver microsomes; MPS1, monopolar spindle 1 kinase; MSD, Meso Scale Discovery; MTT, 3-(4,5-dimethylthiazol-2-yl)-2,5-diphenyltetrazolium bromide; NEK2, NIMA-related kinase 2; PARP, poly ADP ribose polymerase; PLK1, polo-like kinase 1; PTEN, phosphatase and tensin homologue; SAC, spindle assembly checkpoint; TOSMIC, *p*-toluenesulfonylmethyl isocyanide; UDPGA, UDP-glucuronic acid; V_d, volume of distribution

■ REFERENCES

- (1) Hardwick, K. G. The spindle checkpoint. *Trends Genet.* **1998**, *14*, 1–4.
- (2) Musacchio, A.; Salmon, E. D. The spindle-assembly checkpoint in space and time. *Nat. Rev. Mol. Cell Biol.* **2007**, *8*, 379–393.
- (3) Weiss, E.; Winey, M. The *Saccharomyces cerevisiae* spindle pole body duplication gene MPS1 is part of a mitotic checkpoint. *J. Cell Biol.* **1996**, *132*, 111–123.
- (4) Lauze, E.; Stoelcker, B.; Luca, F. C.; Weiss, E.; Schutz, A. R.; Winey, M. Yeast spindle pole body duplication gene MPS1 encodes an essential dual specificity protein kinase. *EMBO J.* **1995**, *14*, 1655–1663.
- (5) Mills, G. B.; Schmandt, R.; McGill, M.; Amendola, A.; Hill, M.; Jacobs, K.; May, C.; Rodricks, A. M.; Campbell, S.; Hogg, D. Expression of TTK, a novel human protein kinase, is associated with cell proliferation. *J. Biol. Chem.* **1992**, *267*, 16000–16006.
- (6) Stucke, V. M.; Sillje, H. H.; Arnaud, L.; Nigg, E. A. Human Mps1 kinase is required for the spindle assembly checkpoint but not for centrosome duplication. *EMBO J.* **2002**, *21*, 1723–1732.
- (7) Mattison, C. P.; Old, W. M.; Steiner, E.; Huneycutt, B. J.; Resing, K. A.; Ahn, N. G.; Winey, M. Mps1 activation loop autophosphorylation enhances kinase activity. *J. Biol. Chem.* **2007**, *282*, 30553–30561.
- (8) Landi, M. T.; Dracheva, T.; Rotunno, M.; Figueroa, J. D.; Liu, H.; Dasgupta, A.; Mann, F. E.; Fukuoka, J.; Hames, M.; Bergen, A. W.; Murphy, S. E.; Yang, P.; Pesatori, A. C.; Consonni, D.; Bertazzi, P. A.; Wacholder, S.; Shih, J. H.; Caporaso, N. E.; Jen, J. Gene expression signature of cigarette smoking and its role in lung adenocarcinoma development and survival. *PLoS One* **2008**, *3*, e1651-1–e1651-8.
- (9) Mizukami, Y.; Kono, K.; Daigo, Y.; Takano, A.; Tsunoda, T.; Kawaguchi, Y.; Nakamura, Y.; Fujii, H. Detection of novel cancer-testis antigen-specific T-cell responses in TIL, regional lymph nodes, and PBL in patients with esophageal squamous cell carcinoma. *Cancer Sci.* **2008**, *99*, 1448–1454.
- (10) Salvatore, G.; Nappi, T. C.; Salerno, P.; Jiang, Y.; Garbi, C.; Ugolini, C.; Miccoli, P.; Basolo, F.; Castellone, M. D.; Cirafici, A. M.; Melillo, R. M.; Fusco, A.; Bittner, M. L.; Santoro, M. A cell proliferation and chromosomal instability signature in anaplastic thyroid carcinoma. *Cancer Res.* **2007**, *67*, 10148–10158.
- (11) Thykjaer, T.; Workman, C.; Kruhoffer, M.; Demtroder, K.; Wolf, H.; Andersen, L. D.; Frederiksen, C. M.; Knudsen, S.; Orntoft, T. F. Identification of gene expression patterns in superficial and invasive human bladder cancer. *Cancer Res.* **2001**, *61*, 2492–2499.
- (12) Yuan, B.; Xu, Y.; Woo, J. H.; Wang, Y.; Bae, Y. K.; Yoon, D. S.; Wersto, R. P.; Tully, E.; Wilsbach, K.; Gabrielson, E. Increased expression of mitotic checkpoint genes in breast cancer cells with chromosomal instability. *Clin. Cancer Res.* **2006**, *12*, 405–410.
- (13) Carter, S. L.; Eklund, A. C.; Kohane, I. S.; Harris, L. N.; Szallasi, Z. A signature of chromosomal instability inferred from gene expression profiles predicts clinical outcome in multiple human cancers. *Nat. Genet.* **2006**, *38*, 1043–1048.
- (14) Brough, R.; Frankum, J. R.; Sims, D.; Mackay, A.; Mendes-Pereira, A. M.; Bajrami, I.; Costa-Cabral, S.; Rafiq, R.; Ahmad, A. S.; Cerone, M. A.; Natrajan, R.; Sharpe, R.; Shiu, K. K.; Wetterskog, D.; Dedes, K. J.; Lambros, M. B.; Rawjee, T.; Linardopoulos, S.; Reis-Filho, J. S.; Turner, N. C.; Lord, C. J.; Ashworth, A. Functional viability profiles of breast cancer. *Cancer Discovery* **2011**, *1*, 260–273.
- (15) Gordon, D. J.; Resio, B.; Pellman, D. Causes and consequences of aneuploidy in cancer. *Nat. Rev. Genet.* **2012**, *13*, 189–203.
- (16) Chu, M. L.; Chavas, L. M.; Douglas, K. T.; Evers, P. A.; Taberner, L. Crystal structure of the catalytic domain of the mitotic checkpoint kinase Mps1 in complex with SP600125. *J. Biol. Chem.* **2008**, *283*, 21495–21500.
- (17) Dorer, R. K.; Zhong, S.; Tallarico, J. A.; Wong, W. H.; Mitchison, T. J.; Murray, A. W. A small-molecule inhibitor of Mps1 blocks the spindle-checkpoint response to a lack of tension on mitotic chromosomes. *Curr. Biol.* **2005**, *15*, 1070–1076.
- (18) Schmidt, M.; Budirahardja, Y.; Klompmaker, R.; Medema, R. H. Ablation of the spindle assembly checkpoint by a compound targeting Mps1. *EMBO Rep.* **2005**, *6*, 866–872.
- (19) Santaguida, S.; Tighe, A.; D'Alise, A. M.; Taylor, S. S.; Musacchio, A. Dissecting the role of MPS1 in chromosome biorientation and the spindle checkpoint through the small molecule inhibitor reversine. *J. Cell Biol.* **2010**, *190*, 73–87.
- (20) Kwiatkowski, N.; Jelluma, N.; Filippakopoulos, P.; Soundararajan, M.; Manak, M. S.; Kwon, M.; Choi, H. G.; Sim, T.; Deveraux, Q. L.; Rottmann, S.; Pellman, D.; Shah, J. V.; Kops, G. J.; Knapp, S.; Gray, N. S. Small-molecule kinase inhibitors provide insight into Mps1 cell cycle function. *Nat. Chem. Biol.* **2010**, *6*, 359–368.
- (21) Lan, W.; Cleveland, D. W. A chemical tool box defines mitotic and interphase roles for Mps1 kinase. *J. Cell Biol.* **2010**, *190*, 21–24.
- (22) Tardif, K. D.; Rogers, A.; Cassiano, J.; Roth, B. L.; Cimbor, D. M.; McKinnon, R.; Peterson, A.; Douce, T. B.; Robinson, R.; Dorweiler, I.; Davis, T.; Hess, M. A.; Ostanin, K.; Papac, D. I.; Baichwal, V.; McAlexander, I.; Willardsen, J. A.; Saunders, M.; Christophe, H.; Kumar, D. V.; Wettstein, D. A.; Carlson, R. O.; Williams, B. L. Characterization of the cellular and antitumor effects of MPI-0479605, a small-molecule inhibitor of the mitotic kinase Mps1. *Mol. Cancer Ther.* **2011**, *10*, 2267–2275.
- (23) Hewitt, L.; Tighe, A.; Santaguida, S.; White, A. M.; Jones, C. D.; Musacchio, A.; Green, S.; Taylor, S. S. Sustained Mps1 activity is required in mitosis to recruit O-Mad2 to the Mad1-C-Mad2 core complex. *J. Cell Biol.* **2010**, *190*, 25–34.
- (24) Caldarelli, M.; Angiolini, M.; Disingrini, T.; Donati, D.; Guanci, M.; Nuvoloni, S.; Poster, H.; Quartieri, F.; Silvagni, M.; Colombo, R. Synthesis and SAR of new pyrazolo[4,3-h]quinazoline-3-carboxamide derivatives as potent and selective MPS1 kinase inhibitors. *Bioorg. Med. Chem. Lett.* **2011**, *21*, 4507–4511.
- (25) Colombo, R.; Caldarelli, M.; Mennecozzi, M.; Giorgini, M. L.; Sola, F.; Cappella, P.; Perrera, C.; Depaolini, S. R.; Rusconi, L.; Cucchi, U.; Avanzi, N.; Bertrand, J. A.; Bossi, R. T.; Pesenti, E.; Galvani, A.; Isacchi, A.; Colotta, F.; Donati, D.; Moll, J. Targeting the mitotic checkpoint for cancer therapy with NMS-P715, an inhibitor of MPS1 kinase. *Cancer Res.* **2010**, *70*, 10255–10264.
- (26) Kusakabe, K.; Ide, N.; Daigo, Y.; Itoh, T.; Higashino, K.; Okano, Y.; Tadano, G.; Tachibana, Y.; Sato, Y.; Inoue, M.; Wada, T.; Iguchi, M.; Kanazawa, T.; Ishioka, Y.; Dohi, K.; Tagashira, S.; Kido, Y.; Sakamoto, S.; Yasuo, K.; Maeda, M.; Yamamoto, T.; Higaki, M.; Endoh, T.; Ueda, K.; Shiota, T.; Murai, H.; Nakamura, Y. Diaminopyridine-based potent and selective Mps1 kinase inhibitors binding to an unusual flipped-peptide conformation. *ACS Med. Chem. Lett.* **2012**, *3*, 560–564.
- (27) Kusakabe, K.; Ide, N.; Daigo, Y.; Tachibana, Y.; Itoh, T.; Yamamoto, T.; Hashizume, H.; Hato, Y.; Higashino, K.; Okano, Y.; Sato, Y.; Inoue, M.; Iguchi, M.; Kanazawa, T.; Ishioka, Y.; Dohi, K.; Kido, Y.; Sakamoto, S.; Yasuo, K.; Maeda, M.; Higaki, M.; Ueda, K.;

Yoshizawa, H.; Baba, Y.; Shiota, T.; Murai, H.; Nakamura, Y. Indazole-based potent and cell-active Mps1 kinase inhibitors: Rational design from pan-kinase inhibitor anthrapyrazolone (SP600125). *J. Med. Chem.* **2013**, *56*, 4343–4356.

(28) Livecchi, M.; Calvet, G.; Schmidt, F. Palladium-catalyzed synthesis of 2,3-disubstituted 5-azaindoles via heteroannulation reaction and of 2-substituted 5-azaindoles through domino Sila-Sonogashira/5-endo cyclization. *J. Org. Chem.* **2012**, *77*, 5006–5016.

(29) Le Brazidec, J. Y.; Pasis, A.; Tam, B.; Boykin, C.; Wang, D.; Marcotte, D. J.; Claassen, G.; Chong, J. H.; Chao, J.; Fan, J.; Nguyen, K.; Silvian, L.; Ling, L.; Zhang, L.; Choi, M.; Teng, M.; Pathan, N.; Zhao, S.; Li, T.; Taveras, A. Structure-based design of 2,6,7-trisubstituted-7H-pyrrolo[2,3-d]pyrimidines as Aurora kinases inhibitors. *Bioorg. Med. Chem. Lett.* **2012**, *22*, 4033–4037.

(30) Hopkins, A. L.; Groom, C. R.; Alex, A. Ligand efficiency: A useful metric for lead selection. *Drug Discovery Today* **2004**, *9*, 430–431.

(31) McNicholas, S.; Potterton, E.; Wilson, K. S.; Noble, M. E. Presenting your structures: The CCP4mg molecular-graphics software. *Acta Crystallogr., Sect. D* **2011**, *67*, 386–394.

(32) Estrada, A. A.; Liu, X.; Baker-Glenn, C.; Beresford, A.; Burdick, D. J.; Chambers, M.; Chan, B. K.; Chen, H.; Ding, X.; DiPasquale, A. G.; Dominguez, S. L.; Dotson, J.; Drummond, J.; Flagella, M.; Flynn, S.; Fujii, R.; Gill, A.; Gunzner-Toste, J.; Harris, S. F.; Heffron, T. P.; Kleinheinz, T.; Lee, D. W.; Le Pichon, C. E.; Lyssikatos, J. P.; Medhurst, A. D.; Moffat, J. G.; Mukund, S.; Nash, K.; Scarce-Levie, K.; Sheng, Z.; Shore, D. G.; Tran, T.; Trivedi, N.; Wang, S.; Zhang, S.; Zhang, X.; Zhao, G.; Zhu, H.; Sweeney, Z. K. Discovery of highly potent, selective, and brain-penetrable leucine-rich repeat kinase 2 (LRRK2) small molecule inhibitors. *J. Med. Chem.* **2012**, *55*, 9416–9433.

(33) Kornev, A. P.; Taylor, S. S.; Ten Eyck, L. F. A helix scaffold for the assembly of active protein kinases. *Proc. Natl. Acad. Sci. U.S.A.* **2008**, *105*, 14377–14382.

(34) Chu, M. L.; Lang, Z.; Chavas, L. M.; Neres, J.; Fedorova, O. S.; Taberner, L.; Cherry, M.; Williams, D. H.; Douglas, K. T.; Evers, P. A. Biophysical and X-ray crystallographic analysis of Mps1 kinase inhibitor complexes. *Biochemistry* **2010**, *49*, 1689–1701.

(35) Workman, P.; Collins, I. Probing the probes: Fitness factors for small molecule tools. *Chem. Biol.* **2010**, *17*, 561–577.

(36) Dou, Z.; von Schubert, C.; Korner, R.; Santamaria, A.; Elowe, S.; Nigg, E. A. Quantitative mass spectrometry analysis reveals similar substrate consensus motif for human Mps1 kinase and Plk1. *PLoS One* **2011**, *6*, e18793-1–e18793-9.

(37) Jelluma, N.; Brenkman, A. B.; McLeod, I.; Yates, J. R., 3rd; Cleveland, D. W.; Medema, R. H.; Kops, G. J. Chromosomal instability by inefficient Mps1 auto-activation due to a weakened mitotic checkpoint and lagging chromosomes. *PLoS One* **2008**, *3*, e2415-1–e2415-8.

(38) Langdon, S. R.; Westwood, I. M.; van Montfort, R. L.; Brown, N.; Blagg, J. Scaffold-focused virtual screening: Prospective application to the discovery of TTK inhibitors. *J. Chem. Inf. Model.* **2013**, *53*, 1100–1112.

(39) Leslie, A. G.; Powell, H. R. Processing diffraction data with Mosflm. In *Evolving Methods for Macromolecular Crystallography*; Read, R. J., Sussman, J. L., Eds.; Springer: New York, 2007; Vol. 245, pp 41–51.

(40) Winn, M. D.; Ballard, C. C.; Cowtan, K. D.; Dodson, E. J.; Emsley, P.; Evans, P. R.; Keegan, R. M.; Krissinel, E. B.; Leslie, A. G.; McCoy, A.; McNicholas, S. J.; Murshudov, G. N.; Pannu, N. S.; Potterton, E. A.; Powell, H. R.; Read, R. J.; Vagin, A.; Wilson, K. S. Overview of the CCP4 suite and current developments. *Acta Crystallogr., Sect. D* **2011**, *67*, 235–242.

(41) Kabsch, W. Xds. *Acta Crystallogr., Sect. D* **2010**, *66*, 125–132.

(42) Evans, P. Scaling and assessment of data quality. *Acta Crystallogr., Sect. D* **2006**, *62*, 72–82.

(43) McCoy, A. J.; Grosse-Kunstleve, R. W.; Adams, P. D.; Winn, M. D.; Storoni, L. C.; Read, R. J. Phaser crystallographic software. *J. Appl. Crystallogr.* **2007**, *40*, 658–674.

(44) Emsley, P.; Cowtan, K. Coot: Model-building tools for molecular graphics. *Acta Crystallogr., Sect. D* **2004**, *60*, 2126–2132.

(45) Bricogne, G.; Blanc, E.; Brandl, M.; Flensburg, C.; Keller, P.; Paciorek, W.; Roversi, P.; Sharff, A.; Smart, O. S.; Vonnrhein, C.; Womack, T. O. BUSTER, version 2.11.4; Global Phasing Ltd.: Cambridge, United Kingdom, 2012.

(46) Smart, O. S.; Womack, T. O.; Sharff, A.; Flensburg, C.; Keller, P.; Paciorek, W.; Vonnrhein, C.; Bricogne, G. *Grade*, version 1.2.1; Global Phasing Ltd.: Cambridge, United Kingdom, 2012.

(47) Bruno, I. J.; Cole, J. C.; Lommerse, R. S.; Rowland, R.; Taylor, R.; Verdonk, M. L. Isostar: A library of information about non-bonded interactions. *J. Comput.-Aided. Mol. Des.* **1997**, *11*, 525–537.

(48) Davis, I. W.; Leaver-Fay, A.; Chen, V. B.; Block, J. N.; Kapral, G. J.; Wang, X.; Murray, L. W.; Arendall, W. B., 3rd; Snoeyink, J.; Richardson, J. S.; Richardson, D. C. MolProbity: All-atom contacts and structure validation for proteins and nucleic acids. *Nucleic Acids Res.* **2007**, *35*, W375–W383.

(49) Workman, P.; Aboagye, E. O.; Balkwill, F.; Balmain, A.; Bruder, G.; Chaplin, D. J.; Double, J. A.; Everitt, J.; Farningham, D. A.; Glennie, M. J.; Kelland, L. R.; Robinson, V.; Stratford, I. J.; Tozer, G. M.; Watson, S.; Wedge, S. R.; Eccles, S. A. Guidelines for the welfare and use of animals in cancer research. *Br. J. Cancer* **2010**, *102*, 1555–1577.